Maxwell Joel Mageto

TEM STUDY OF MICROSTRUCTURE IN RELATION TO HARDNESS AND DUCTILITY IN Al-Mg-Si (6xxx) ALLOYS

MSc Thesis

Department of Physics

Faculty of Natural Sciences and Technology

Norwegian University of Science and Technology (NTNU)

N-7491 Trondheim

Norway.

Norwegian University of Science and Technology - NTNU
Faculty of Natural Science and Technology
Department of Physics

MASTER OF SCIENCE (PHYSICS) THESIS FOR

MSC. STUDENT: MAXWELL JOEL MAGETO

Thesis started: 01.10.2002
Thesis submitted: 18.06.2003

DISCIPLINE: MATERIALS PHYSICS

English title: TEM studies of microstructure in relation to hardness and ductility in Al-Mg-Si (6xxx) alloys

This work has been carried out at the Department of Physics under the supervision of Research Scientist Dr. Calin Marioara, SINTEF Materials Technology and Professor Randi Holmestad, NTNU.

Trondheim, 17. June 2003

Randi Holmestad
Responsible supervisor
Professor at Department of Physics

Abstract

Two different solution heat treatments (2hours at 570°C and 10minutes at 520°C) have been used to study precipitation in two 6xxx (Al-Mg-si) dispersoid-free-alloys with composition: 0.721 at % Si, 0.577 at % Mg (alloy A3) and 0.57 at %Si 0.72 at % Mg (alloy A12). The relation between their microstructure and macroscopical properties such as hardness and ductility has been investigated. Tensile tests, hardness measurements, electrical conductivity sigma tests, grain size measurements in optical microscope and microstructure characterization in Transmission Electron Microscope (TEM) have all been done. The effect of alloy composition and solution heat treatment temperature and time on the microstructure and the resulting macroscopical properties (hardness, yield stress, tensile strength and ductility) was investigated. The results indicate that when alloy A3 is solution treated at 520°C for 10 minutes and then annealed for 3 hours at 175°C, its hardness, yield stress and tensile strength as well as ductility is optimised i.e.A3 has better mechanical properties and low cost of production at these conditions. It has been proved that the strengthening was solely due to precipitation particles and not grain size.

Summary

Precipitation strengthened Al alloys are used extensively in the aircraft industry e.g. 6061 (Al-Mg-Si) is used in wing spars and plane skins. The alloys of 6XXX series are applied in heavy duty structures in rail coaches, truck frames, ship building, bridges, boiler making, hydraulic systems, mining equipment, pylons and towers, motorboats, frame work for tents, rivets etc. They are used for structural applications due to their low density, strength, recyclability without loss of quality, corrosion resistance, durability, ductility, formability and conductivity. The technological applications of these alloys continue to increase hence the need for alloy improvement. The previous study and research on precipitation hardening Al-Mg-Si (6XXX) alloys indicate that their strength and properties are achieved by heat treatments of varying complexity and alloy design.

The main characteristic of the 6xxx alloys is the tremendous increase in hardness, due to the precipitation of Mg-Si metastable phases upon annealing at intermediate temperatures. Previous research has shown that the main hardening phase is β", for alloys whose Si/Mg ratio is approximately 1. The β" phase exists in the form of needles oriented parallel with the three <100> directions in the Al matrix.

The purpose of this M.Sc. degree thesis has been to understand the effect of solution heat temperature and time, alloy composition and annealing time on microstructure and the resulting macroscopical properties in order to optimise Aluminium-Magnesium-Silicon alloys for the desired industrial application. . This thesis work is therefore concerned with the strengthening and ductility, which results from two different heat treatments subjected on two Al-Mg-Si alloys and how these (strength and ductility) depend on the nature of precipitates formed. Thus the scope of this work is limited to the main hardening phases:- Gp-zones

and β" precipitates. Two different solution heat treatments (2hours at 570°C and 10minutes at 520°C) have been used to study precipitation in two 6xxx (Al-Mg-si) dispersoid-free-alloys with composition: 0.721 at % Si, 0.577 at % Mg (alloy A3) and 0.57 at %Si 0.72 at % Mg (alloy A12). Immediately after solution heat treatment, the alloys were quenched and aged for 0.5 to 200 hours at 175°C. This isothermal ageing temperature is commonly used in industry and causes β" to precipitate. β" is the most efficient hardening phase in the 6xxx aluminium alloy system and forms at temperatures between 125°C and 200°C. The relation between their microstructure and macroscopical properties such as hardness, yield strength, tensile strength and ductility has been investigated. Tensile tests, hardness measurements, electrical conductivity sigma tests, grain size measurements in optical microscope and microstructure characterization in Transmission Electron Microscope (TEM) have all been done.

The main instrumentation used in the analysis has been the Transmission Electron Microscope (TEM). Conventional TEM techniques were employed for purposes of visualizing the particles by contrast imaging. Thickness of foil determination that was used in computing volume density calculations was performed with Parallel Electron Energy Loss Spectrometer (PEELS). Mechanical tensile testing was carried out in an Instron tensile testing machine model No 1125.

This thesis is divided into four parts. The first part gives a general introduction including classification of Al alloys and their practical uses and factors affecting microstructure and mechanical properties. The second part contains the mechanism in age hardening alloys and the principles of electron microscopy. It also explores the hardening mechanisms, tensile properties, electrical conductivity and grains. Part three presents the experimental techniques used including

apparatus used and the procedure followed. Part four presents the results and discussions. Part five attempts to give the main conclusions drawn.

The results indicate that when alloy A3 (Si-rich alloy) is solution treated at 520°C for 10 minutes and then annealed for 3 hours at 175°C, its hardness, yield stress and tensile strength as well as ductility is optimised i.e.A3 has better mechanical properties and low cost of production at these conditions.

Table of Contents

Abstract iii
List of figures x
Acknowledgments xiii
Abbreviations xiv

1 Chapter 1 **GENERAL INTRODUCTION** 1
1.1 Purpose and Scope 3
1.1.1 The specific objectives included:- 4
1.2 Effect of atomic arrangement and the microstructure of metals upon their physical properties 4
1.3 Aluminium Alloys 5
1.4 Why study aluminium alloys? 7

2 Chapter 2 **THEORY** 10
2.1 Introduction to precipitation in Age Hardenable Alloys 10
2.1.1 Precipitation Hardening 11
2.1.2 Basic Requirements for Ageing 11
2.2 Stages of Heat Treatment 13
2.2.1 Solution Heat Treatment 13
2.2.2 Quenching 13
2.2.3 Ageing 14
2.2.4 The Al-Cu precipitation sequence 16
2.2.5 GP Zones 17
2.3 Precipitation in Al-Mg-Si (6XXX) Alloys 18
2.4 Vacancies 20
2.5 Structure of GP zones and β" in Al-Mg-Si alloys. 22
2.6 Hardening Mechanisms 25
2.6.1 Coherency strain hardening 25
2.6.2 Chemical hardening 26
2.6.3 Dispersion Hardening 26
2.6.4 The ageing Curve for Aluminium alloys 27
2.7 Tensile properties 28
2.8 Engineering Stress and Engineering Strain 29
2.8.1 Tensile strength 31
2.8.2 Elastic limit: 34

2.9 Grains 34
2.10 Electrical Conductivity 35
2.11 Eddy Current 36
2.12 Transmission Electron Microscopy 37
2.12.1 Electron Diffraction 40
2.12.2 Diffraction Patterns, Bright Field and Dark Field 40
2.12.3 Electron Energy Loss Spectroscopy (EELS) 42

3 Chapter 3 **EXPERIMENTAL TECHNIQUES** 44
3.1.1 Sample Preparation 44
3.2 Heat Treatment 45
3.3 Grain size specimen preparation and measurement 48
3.4 Hardness Measurements 49
3.5 Electrical conductivity 50
3.6 The Tensile Test 51
3.7 TEM specimen preparation 52
3.8 Microscopy and EELS 53
3.9 Measurement of Microstructure 53
3.9.1 Length of the needles (L) 53
3.9.2 Number density (N) 54
3.9.3 Cross Section area (CS) 54
3.9.4 Particle Density (ρ) 55
3.9.5 Volume Fraction (VF) 55

4 CHAPTER 4 **RESULTS AND DISCUSSION** 56
4.1 Grain Size 56
4.2 Tables of Experimental results 61
4.3 Graphs 64
4.3.1 Ageing at Room temperature Curve 64
4.3.2 Hardness Curves 65
4.3.3 Electrical Conductivity curves 66
4.3.4 Stress-strain Curves for investigated alloys 67
4.3.5 Stress-strain curve for AA6082 68
4.4 Microstructural Examination by TEM 68
4.5 Hardness 75
4.6 Tensile Stress-Strain Behaviour 81
4.7 Electrical Conductivity 86

5 Chapter 5 **CONCLUSIONS AND SUGGESTIONS FOR FURTHER WORK** 88
5.1 Conclusions 88

5.2 Suggestions for further work 89

6 **Bibliography** 91

7 **APPENDIX** 92
7.1 The Al-Mg-Si Phase digram for Homogenanization 92
7.2 **GLOSSARY** 93
7.3 Data from tensile test 95

List of figures

Figure 1-1 Processing-Structure-Properties Relationship [12] 1
Figure 2-1 Age hardening heat treatment binary phase diagram [14] 12
Figure 2-2 Changes in microstructure as a result of quenching [14] 12
Figure 2-3 A general model for the decomposition of a SSSS [10] 15
Figure 2-4 Phase diagram of a Al-Cu alloy 16
Figure 2-5 Equilibrium Concentration of Vacancies 21
Figure 2-6 Vickers Hardness curve 22
Figure 2-7 HREM images of (a) β" and (b) GP zone 24
Figure 2-8 various precipitate-matrix interfaces [21]. 25
Figure 2-9 Ordered particles 26
Figure 2-10 Dislocations (Orowan looping) [2] 27
Figure 2-11 Ageing curve for Al Allloys. 27
Figure 2-12 Cylindrical bar subjected to axial load 29
Figure 2-13 Stress – Strain curves 33
Figure 2-14 Eddy Current demonstration 36
Figure 2-15 Schematic view of electron optics in the TEM column [1] 37
Figure 2-16 Electron beam and Specimen interaction 39
Figure 2-17 The Bragg description of diffraction 40
Figure 2-18 Bright field and a dark field image [9] 41
Figure 2-19 EELS spectrum. 42
Figure 3-1 Cutting of alloy specimens 45
Figure 3-2 Heat treatment (i) 45
Figure 3-3 Heat treatment (ii) 46
Figure 3-4 Measurement of grain diameter by intercept method 48
Figure 3-5 Vickers Hardness Test 50
Figure 3-6 Tensile test specimen 51
Figure 4-1 Micrographs of the as-extruded-grains of alloys A12 and A3 56
Figure 4-2 Figure showing the orientation of grain size measurement. 57
Figure 4-3 Micrographs of the grains of A12/520/17h 57
Figure 4-4 Micrographs of the grains of A3/520/17h 57
Figure 4-5 Micrographs of the grains of A3/570/17h 58
Figure 4-6 Micrographs of the grains of A12/570/17h 58
Figure 4-7 Micrographs of the grains of A12/570/3h 58
Figure 4-8 Micrographs of the grains of A12/520/3h 59
Figure 4-9 Micrographs of the grains of A3/570/3h 59
Figure 4-10 Micrographs of the grains of A3/520/3h 60
Figure 4-11 Ageing behaviour at room temperature 64
Figure 4-12 Vickers Hardness curves 65
Figure 4-13 Electrical Conductivity curves 66

Figure 4-14 Stress – Strain curves 67
Figure 4-15 Stress-Strain Curve for a T4 AA6082 Alloy 68
Figure 4-16 TEM bright field images of A3/520/3h.....69
Figure 4-17 TEM bright field images of A12/570/3h.....70
Figure 4-18 TEM bright field images of A12/520 °C /17h 71
Figure 4-19 TEM bright field images of A12/570/17h 72
Figure 4-20 β" precipitates in A3/520/17h 73
Figure 4-21 β" phase magnified from box in Figure 4-20 73
Figure 4-22 Different phases observed in A12/570/17hr 73
Figure 4-23 Effect of composition and aging time on density of β" 78
Figure 7-1 Solid Solubility limits for Al-Mg-Si [19] 92

List of tables

Table 1-1 Effect of microstructure upon their physical properties [2, p.2] 5
Table 1-2 Classification of Aluminium alloys.....6
Table 1-3 letters designating temper.....6
Table 1-4 Products made from aluminium/ aluminium alloys.....9
Table 2-1 Precipitates of the Al-Mg-Si alloy precipitation sequence 19
Table 3-1 Composition of the investigated alloys.....44
Table 3-2 Heat treatment and sample description.....47
Table 4-1 Data for Grain Size measurements 61
Table 4-2 Mean values of Vickers Hardness after ageing at 175 °C 63
Table 4-3 Results of the mean values of electrical conductivity.....63
Table 4-4 particle densities and Volume Fractions.....74
Table 4-5 Tensile Test Results of specimen A3 and A12.....82
Table 7-1 Tensile data.....95

Acknowledgments

This project has been carried out at the Norwegian University of Science and Technology (NTNU), in cooperation with the department Materials Technology/Metallurgy and the department of Physics, during the period between October 2002 and June 2003. My supervisors through out this work have been Prof. Randi Holmestad of Physics department and and Dr. Calin Daniel Marioara of Sintef Materials Technology, applied Physics..

The author wishes to take this opportunity to thank the supervisors for their relentless support, enthusiasm and interest through out my entire period of doing research pertaining to this work. Their intellect, wisdom and patience gave me all the zeal to push forward with the project.

The author wishes also to thank Pål Ulseth for providing unfailing initial help, an enabling environment and experimental apparatus for heat treatmens, grain size measurements and tensile test. My gratitudes are due to Dr Marioara for his input, knowledge imparted to me and help with microscopy. I am very grateful to Prof. Randi for her experimental guidance. Through out the research period, she was cooperative, helpful and instrumental in making sure everything went on smoothly. Her weekly meetings/discussions with me were very essential and served as an impetus to completing this huge amount of work in time. She provided me with everything I needed.

Maxwell Joel Mageto, B.Ed(Sc.) Hons

Abbreviations

BF: Bright Field

DF: Dark Field

DP: Diffraction Pattern

e : Tensile strain

σ : Stress

σ_y : Yield Stress

E: Young's Modulus

J: Current Density

HV: Vickers Hardness

PEELS: Parallel Electron Energy Loss Spectrometer

RT: Room Temperature

SSSS: Super Saturated Solid Solution

TEM: Transmission Electron Microscope(y)

UTS: Ultimate Tensile Stress

TS: Tensile Stress

APFIM Atom Probe Field Ion Microscopy

A3/520/3h Alloy A3 solution treated for 10minutes at 520°C, quenched and stored for 4 hours at room temperature before being aged for 3hours at 175°C

A12/570/17 Alloy A12 solution treated for 2 hours at 570°C, quenced and stored for 4 hours at room temperature before being aged for 17 hours at 175°C

1 Chapter 1 GENERAL INTRODUCTION

The mechanical properties (hardness, tensile strength, Yield strength, ductility etc) and physical properties (density, electrical and thermal conductivities etc) and microstructure of age harden-able alloys can be very significantly altered with addition of small alloying elements and by suitable heat treatment (homogenisation temperature, ageing temperature, annealing time, storage time at room temperature, heating/cooling rates etc) ([3],[10]). That means the external parameters:- heat treatment , alloy composition etc can change the internal parameters i.e. the microstructure and hence macroscopic properties of a material as is illustrated by the diagram below.

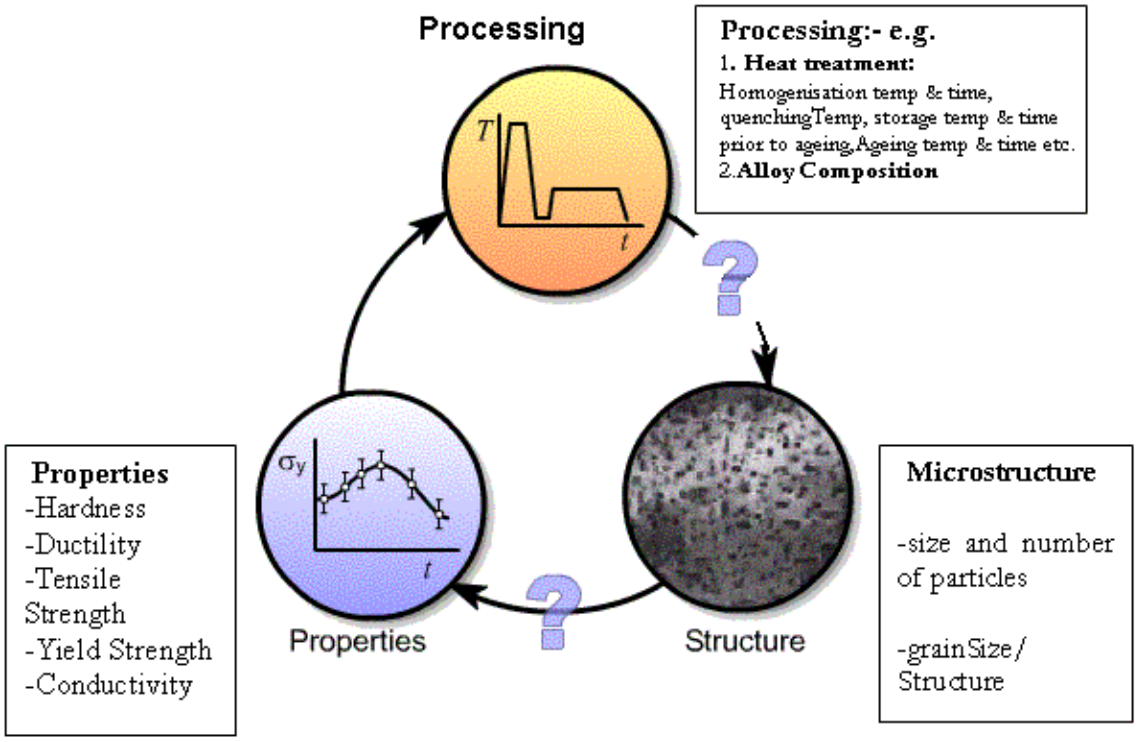

Figure 1-1 Processing-Structure-Properties Relationship [12]

The ideal microstructure depends on the particular application for which the material will be used. The designer may have to consider strength, fracture toughness, fatigue resistance, stiffness, ductility, conductivity, hardness, environmental sensitivity or combinations of these

properties. For many applications the strongest alloy that meets the minimum requirements for other properties is usually selected., the main focus therefore for designers and scientists is developing a microstructure[1] that produces high strength[13]. In order to achieve high strength, the microstructure should be tailored to inhibit slip, i.e. the microstructional feature should be that of strong obstacles [2]. For the case of electrical conductivity, the microstructure should minimize scattering of conductor electrons i.e. should be a pure metal or a small volume fraction of strain-free particles [13]. The microstructure of an alloy is described by identification of the types of phases present and description of their shape and size distributions ([1],[3]).

For 6xxx alloys (see classification of Al alloys Table 1-2), Heat treatment is used to promote the formation of needle shaped precipitates from the SSSS (see stages of heat treatment in section 2.2) of Mg and Si in Al to achieve appreciable mechanical properties. The type of precipitate that gives rise to the maximum strength of 6xxx alloys in the T6 condition is designated β" .The precipitates are fine needles about 30nm long lying parallel to the <001> direction of the matrix. At longer aging times the material loses strength again. This is explained by the coarsening of the hardening phase and the transformation into other Mg-Si phases.

In an attempt to optimise various age harden-able alloys for correct applications, researchers try to fully understand how the alloy composition and heat treatment parameters influence the microstructure and also how the microstructure in turn affects the macroscopical properties.

[1] It is now possible to tailor the microstructure of materials to achieve specific sets of properties; the extraordinary ability of modern TEM

The most important parameters that influence the microstructure and mechanical properties are :-

- Homogenisation temperature,
- Cooling and heating rates,
- Alloy composition and
- Ageing Temperature
- Annealing time
- Mechanical deformation

1.1 Purpose and Scope

The purpose of this M.Sc. degree thesis has been to understand the effect of some of the above parameters (solution heat temperature and time, alloy composition, annealing time) on microstructure and the resulting macroscopical properties in order to optimise Aluminium-Magnesium-Silicon alloys for the desired industrial application. This thesis work is therefore concerned with the strengthening and ductility, which results from different heat treatments of two Al-Mg-Si alloys and how these (strength and ductility) depend on the nature of precipitates formed. The study of precipitation hardening Al-Mg-Si(6XXX) alloys, where the strength and properties are achieved by heat treatments of varying complexity, and alloy design is considered in detail. The Transmission Electron Microscope (TEM) was used to study precipitates in these alloys and to understand their physical macroscopical properties such as hardness, electrical conductivity and ductility in terms of their microstructure. It is clear that because precipitation is controlled by the rate of atomic migration in these alloys, temperature will have a pronounced effect on the process. Furthermore, since precipitation is a thermally activated process, other variables such as introduction of *vacancies by solution treatment, grain size and prior cold work are also important.* Hence the grain size of the specimens has also been investigated in the present work.

In this investigation, an isothermal ageing temperature of 175°C has been used. This temperature is commonly used in industry and causes β" to precipitate. β" is the most efficient hardening phase in the 6xxx aluminium alloy system and forms at temperatures between 125°C and 200°C [3].

This study was undertaken as part of the on-going research programme KMB "Heat Treatment Fundamentals" a joint venture between the Norwegian University of Science and Technology (NTNU) and SINTEF Materials Technology and other interested parties from the Norwegian Industry.

1.1.1 The specific objectives included:-

- To study the Influence of Alloy composition on microstructure and mechanical properties (i.e. hardness and ductility)
- To determine the influence of solution heat treatment conditions on microstructure and mechanical properties (hardness and ductility)
- To investigate the effect of annealing time on microstructure and mechanical properties (hardness and ductility).

1.2 Effect of atomic arrangement and the microstructure of metals upon their physical properties

The mechanical and physical properties of metals are influenced by both the microstructure of the metals and the atom arrangement in the metal as shown in Table 1-1([1] , [2])

Table 1-1 Effect of microstructure of metals upon their physical properties [2, p.2]

Physical Property		Influence of Atomic arrangement And Defects	Influence of Microstructure
Mechanical	1. Strength 2. Ductility	Very strong	Very strong
Electrical and Thermal	1. Resistivity 2. Magnetisation 3.Thermal conductivity	Slight	Slight → Strong

Hence, by control of the atomic arrangement and the microstructure (through casting, working and heat treatment) one may exercise some control over all the physical properties of a metal, but particularly its mechanical properties. ([1], [2], [3]). Knowledge of mechanical and physical properties is important for the correct application of metals [2]. The most useful tool for characterizing microstructure is the optical microscope. Two other very useful microscopes that characterize microstructures of much finer details than is possible with the optical microscope are the Transmission Electron Microscope (TEM) and the Scanning Electron Microscope (SEM) ([1], [2], [3], [4]). A brief introduction to the principles of the TEM is presented in chapter 2 section 2.12 on page 37.

1.3 Aluminium Alloys

Aluminium and its alloys are characterized by a relatively low density, high electrical and thermal conductivities, and a resistance to corrosion ([1],[2],[3]). Many of these alloys are formed by virtue of high ductility [3]. Its ductility is maintained even at very low temperatures. The primary limitation of aluminium is its low melting temperature (660^{o}C). Mechanical strength of aluminium can be enhanced by cold work and by alloying ([2], [3]). However, both processes tend to diminish the resistance to corrosion. Principal alloying elements are copper,

magnesium, silicon, manganese and zinc. A four-digit number that indicates the principal impurities designates composition of aluminium.

The numbering system designates the series as shown below:

Table 1-2 Classification of Aluminium alloys

Material	Designation
Aluminium of 99% minimum purity	1xxx
Aluminium-Copper alloys	2xxx
Aluminium-Manganese alloys	3xxx
Aluminium-Silicon alloys	4xxx
Aluminium-Magnesium alloys	5xxx
Aluminium-Magnesium- silicon alloys	6xxx
Aluminium-Zinc alloys	7xxx
Miscellaneous alloys e.g. aluminium-lithium alloys	8xxx

The American Standards Association has approved a system of letters and numbers to indicate temper. In this system a letter designates the basic temper, whereas modification of the temper is indicated with a number.

Table 1-3 letters designating temper

Symbol	Meaning
O	Annealed
F	As-fabricated
H	Strain hardened
T	Heat treated

T indicates the heat treatment and the number that follows T indicates the modification on the heat treatment process. Examples: T2 = Annealed, T3=Solution heat-treated and cold worked, T4=Solution heat-treated and naturally aged, T6=Solution heat-treated and artificially aged.

1.4 Why study aluminium alloys?

The ability to predict the desired microstructure is central to developing materials that achieve proper levels of performance. Furthermore a thorough knowledge of mechanical and physical properties is very important for correct applications of aluminium alloys. Therefore, a proper understanding of the various structure-property relationships is very crucial in the identification of cost effective solutions and highlighting important objectives in the control of microstructure, the design of aluminium components and their various alloy design with a view to optimizing their mechanical properties. Owing to their diverse applications, we should be concerned with how their structure is controlled; also, the way structure controls the mechanical properties of aluminium alloys. A few examples below will emphasize the need for continuous research of Al and Al alloys. Through continuous research, a detailed understanding of precipitation in Al alloys will allow microstructures of conventionally produced alloys to be controlled so that some service properties can be optimised. This is the justification of undertaking the present investigation.

1. According to the European Aluminium Association: An average European car currently contains a variety of Al components amounting to 65 kg (6% of total car weight)

- Gear box housings
- Cylinder heads
- Wheels
- Radiators
- Bumpers
- Seat rails
- Side impact cars

The use of aluminium in vehicles reduces dead weight and energy consumption while increasing load capacity. Its strength can be adapted to the application required by modifying the composition of its alloys and by various thermal and mechanical treatments.

2. Because of its lightweight, it is the leading material for structures in Aircrafts and high-speed trains. Precipitation strengthened Al alloys are used extensively in the aircraft industry e.g. 6061 (Al-Mg-Si) used in wing spars and plane skins. It is used for structural applications due to moderate strength and corrosion resistant properties [12].

3. More than 90% of the extruded aluminium goods in Western Europe are based on 6XXX series [14]. In particular, the 6XXX series are applied in heavy duty structures in rail coaches, truck frames, ship building, bridges, boiler making, hydraulic systems, mining equipment, pylons and towers, motorboats, frame work for tents, rivets etc.[12]

4. The technological applications of aluminium/aluminium alloys continues to increase because Al is a valuable material owing to its unique properties such as its low density, strength, recyclability without loss of quality, corrosion resistance, durability, ductility, formability and conductivity. Hence the need to study Al and its alloys. Table 1-4 lists a few applications of Al and Aluminium alloys.

Table 1-4 Products made from aluminium/ aluminium alloys

Building:	**Packaging**	**Others**
– Panels – Roofing /ceilings – Windows/doors – Rainwater gutters – Roller shutter doors – Floor heating – Insulation and ventilation	– Food cans – Can bodies – Closures and caps – Container foil – Barrets, flasks and drums	– Mult-layer tubes – Anodising quality – Sanitary applications – Cables for power transmission lines – Reflectors in e.g. rescue blankets and light fittings

Transportation/Automotive	**House-hold related**
– Automotive trim – Heat exchangers – Cycles and invalid chairs – Motor cycles and mopeds – Structural parts – Heat shields – Aircrafts – High speed trains	– Baking trays – Cookware – Domestic machines – Furniture and office equipment – Ladders – Vacuum cleaners – Lighting (surface critical products) – Sports equipment

2 Chapter 2 THEORY

The introduction of a material which possesses considerable strength at both room temperature and elevated temperatures is of great practical importance. It is well known that alloying and cold working can give rise to an increased yield stress, but in certain alloy systems it is possible to produce additional increase in hardness by heat treatment alone [3]. Such a method has many advantages since the required strength can be induced at the most convenient production stage of the heat treatment and fabrication schedule.

The basic requirement for such a special alloy is that it should undergo phase transformation in the solid state.[2]. One hardening reaction commonly used is precipitation from super-saturated solid solution.

2.1 Introduction to precipitation in Age Hardenable Alloys

Precipitation hardening was discovered by accident in 1906 by Wilm [1]. While carrying out experiments to investigate the solid solution strengthening of Mg additions to an Al-Cu-Mn alloy, he accidentally found out that aging a quenched alloy caused a significant increase in hardness. It was not possible for Wilm to observe microstructural changes during the strengthening period at the time since TEM was not yet invented. Therefore the source of the increased strength remained a mystery. Wilm's alloy was first produced in 1909 under the trade name DURALUMINIUM. In 1920, P. D. Merica correctly postulated that the strengthening was due to the formation of submicroscopic particles (precipitates) created at temperatures below the solvus line in the relevant equilibrium phase diagram[3]. However, it was not until the development of the TEM in the 1950's that the nature of the precipitation formation became physically clear, and a more intimate description of the microstructure could be given.

2.1.1 Precipitation Hardening

As pointed out by Prof. Ryum [13] an appealing and simple criterion for a ternary alloy with age-hardening potential is that one of the alloying elements should have a larger atomic radius than Al while the other element should have a smaller atomic radius than Al. Therefore it is anticipated that pairs of Si and Mg atoms would reduce the distortion that each one would cause separately, induce short range order and stabilize Mg-Si clusters since the volume strain would be reduced. The clusters(embryos) should be able to grow to the critical size.

Precipitation hardening, or age hardening is produced by solution treating and quenching an alloy in which a second phase is in solid solution at the elevated temperature but precipitates upon quenching and aging at a lower temperature. The strongest aluminium alloys (2xxx, 6xxx and 7xxx) are produced by precipitation (or age) hardening. In this section, I present how a fine dispersion of precipitates can be formed by appropriate heat treatment.

2.1.2 Basic Requirements for Ageing

The main requirement for an alloy system to respond to age hardening is a significant decrease in solid solubility of one or more of the alloying elements with decreasing temperature. Figure 2-1 shows the solubility line PS, which indicates a decrease in solubility of the θ-phase in the α-phase as the temperature decreases i.e. the solubility of Cu is high at eutectic temperature and decreases rapidly at lower temperature. Usually there is atomic matching, or *coherency,* between the lattices of the precipitate and the matrix. The requirement of a decreasing solubility with temperature places a limitation on the number of useful precipitation-alloy systems.

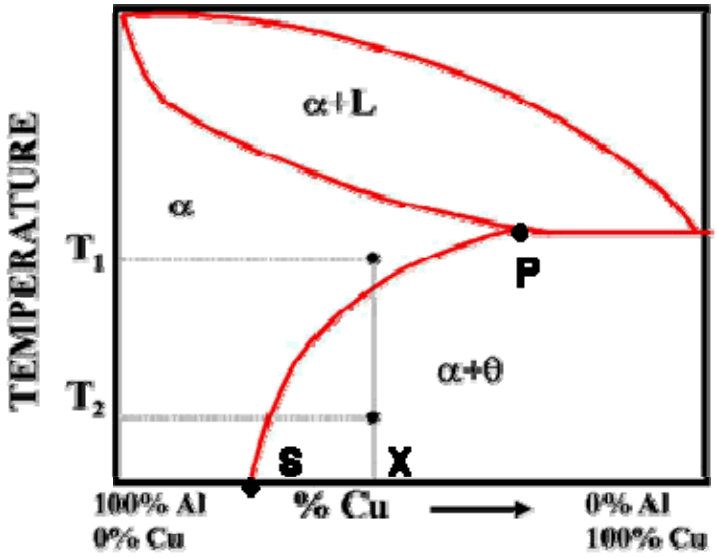

Figure 2-1 Age hardening heat treatment binary phase diagram [14]

At the temperature T_1 the alloy is 100% α, which means that all the constituents are in solid solution

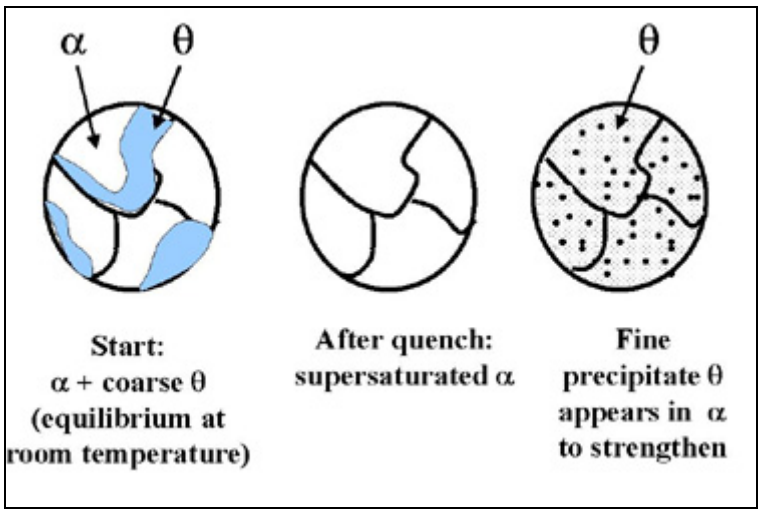

Figure 2-2 Changes in microstructure as a result of quenching [14]

2.2 Stages of Heat Treatment

As indicated above, heat treatment usually comprises 3 main stages, namely Solution heat treatment, quenching and ageing. These stages are described below:

2.2.1 Solution Heat Treatment

In Figure 2-1 above, if an alloy with composition X is heated above the solubility line, PS, to a temperature T1, the θ-phase will dissolve and uniformly disperse into the homogeneous solid α - solution (matrix). Upon slow cooling, the θ-phase would nucleate and grow at heterogeneous sites to form an equilibrium α+θ structure i.e. the phase will reform, and below PS solubility line the metal will once again consist of 2 distinct phases, θ and α. However if the alloy with composition X is heated to temperature, T1, and subsequently quenched in water, the dispersed sub-microscopic phase is trapped in the α-solution. The solution α-phase is said to be supersaturated, because it contains more θ-particles at room temperature than it can hold in its lattice structure. This process is called solution heat treatment. Therefore solution heat treatment is done at a higher temperature within the single-phase region, so as to dissolve the alloying elements.

2.2.2 Quenching

Quenching is done to form a supersaturated solid solution (SSSS) of θ elements in α, and it also reduces the time for diffusion and effectively 'freezes in' the non-equilibrium α - phase structure. Quenching also 'traps' a large amount of vacancies that are created as a result of high temperatures. Equilibrium vacancy concentration increases exponentially with temperature (see Figure 2-5) so that when the alloy is quenched, a super-saturation of vacancies is also frozen into the structure. This has very important implications during any subsequent ageing process.

2.2.3 Ageing

The SSSS is very unstable and if, left alone, the excess θ will precipitate out of the α-phase. This process is called ageing i.e. the controlled decomposition of the supersaturated solid solution to form a fine dispersion of precipitates. This can occur at any temperature below the solvus, even at room temperature. Upon ageing, a SSSS will tend to transform towards the equilibrium structure. However, before equilibrium is attained, a number of intermediate stages (phases) typically occurs [10]. During ageing, precipitation of other phases other than θ (see Figure 2-3) occur, the so-called metastable phases. These are the precipitates that lead to the large strengthening effects termed precipitation hardening. All the precipitate transformations taking place in the alloy from the SSSS until the equilibrium condition is reached are referred to as the precipitation sequence. A typical decomposition sequence is presented in Figure 2-3.

Types of ageing include: -

Natural ageing: when the process occurs at room temperature, it is called natural ageing.

Artificial ageing if the alloy that has been solution heat-treated requires a heating (at a temperature below T2) speed up the precipitation, the process is called artificial ageing.

Abnormal ageing in many instances aging will occur without precipitation. The particle may actually diffuse within the lattices and distort them. This type of ageing is called abnormal aging.

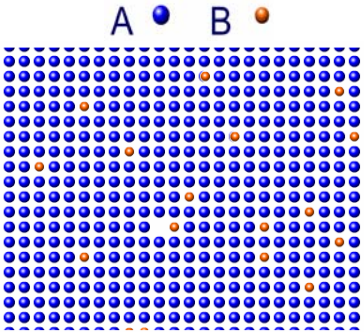

SSSS of B in A, having been formed by quenching from the solution treatment temperature. Note also the presence of 'vacancies', which have been 'frozen in' during the quench.

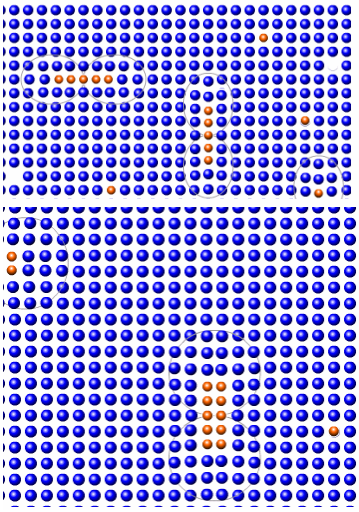

GP zones:
Diffusion during ageing results in localized concentrations of B atoms on specific planes of the A lattice. These are known as GP (Guinier-Preston) zones. In some systems GP zones are disk shaped while others they can be rods, needles or spheres.

Intermediate Stage 2:
GP zones may then provide nucleation sites for a coherent intermediate phase. The A atoms round this plane must then distort even further to accommodate the new phase leading to coherency strain.

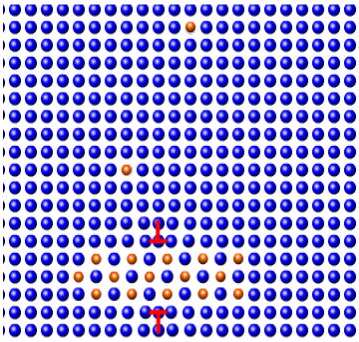

Intermediate stage 3:
As precipitates become larger, some of the coherency strain may be relieved by the formation of dislocations at the interphase. Such precipitates are known as 'semi-coherent'.

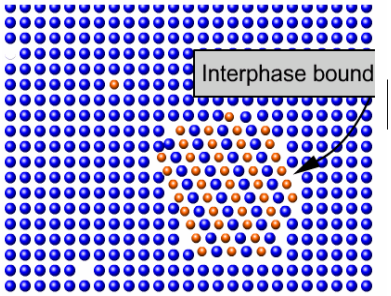

Equilibrium Phase: Is formed after sufficient ageing. This has a different crystal structure from the matrix ('A' atoms) and is normally incoherent with it. There is however a new interphase boundary between the matrix and the precipitate.
.

Figure 2-3 A general model for the decomposition of a SSSS [10]

2.2.4 The Al-Cu precipitation sequence

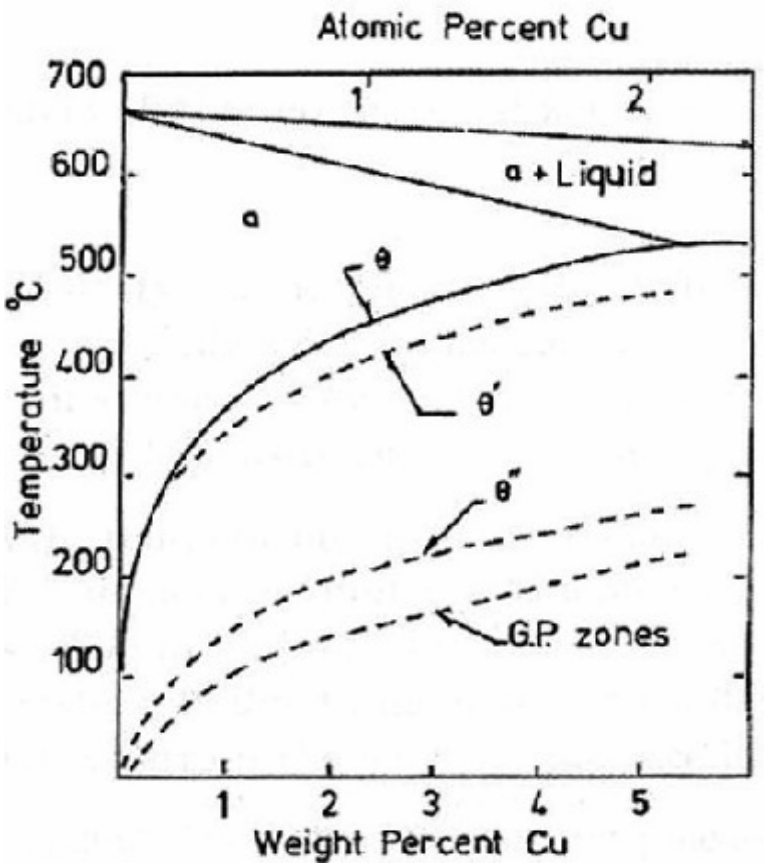

Figure 2-4 Phase diagram illustrating the formation of metastable precipitates in a Al-Cu alloy. Broken lines indicate metastable precipitate phases [1].

The formation of a coherent precipitate in a precipitation-hardening system such as Al-Cu, occurs in a number of steps. After quenching from solid solution the alloy contains regions of solute segregation, or clustering. Guiner and Preston first detected this local clustering with special X-ray techniques, and therefore this structure is known as GP zone. The clustering may produce local strain, so that the hardness of GP[(1)] is higher than for the solid solution.

2.2.5 GP Zones

GP zones are the first precipitates to form upon ageing. They are said to be totally coherent with the Al-matrix. By coherent it is meant that even though the atoms are still in a state of solid solution they have diffused to zones where they imprint their own order on the Al host lattice. It is their number density together with interface strain that gives a high contribution to the strength [3]. The morphology of the GP zones depends on an alloy system for example; they are needles in Al-Mg-Si and spheroids in Al-Mg-Zn or disks in Al-Cu [3]. Although θ is the equilibrium phase in the Al-Cu alloy system, the fully coherent GP zones are the first to precipitate and to nucleate at temperatures below 185ºC. Why ? The main reason for this is embodied in the relative activation energy for nucleation. Being fully coherent with the matrix, GP zones therefore have a very low interfacial energy, the θ phase has a complex tetragonal crystal structure, which can only form with a high energy incoherent interfaces. Further more, GP zones minimize their strain energy by choosing a disc-shape orthogonal to the elastically soft <100> directions in the fcc matrix. Hence despite the fact that the driving force for precipitation of GP zones is less than that for the equilibrium phase, the barrier to nucleation is even smaller, and the zones nucleate quickest. Refer to HREM image of a GP zone of Al-Mg-Si alloys in Figure 2-7 page 24.

With additional aging the hardness is increased further by the ordering of larger clumps of Cu atoms on the {100} planes of the matrix. This structure is known as GP [(2)], or θ''. Next, definite precipitate platelets of $CuAl_2$, or θ', which are coherent with the matrix, form on the {100} planes of the matrix. The coherent precipitate produces an increased strain field in the matrix and a further increase in hardness. With still further ageing the equilibrium phase $CuAl_2$, or θ, is formed from the transition lattice θ''. These particles are no longer coherent with the matrix, and therefore the hardness is lower than at the stage when coherent θ' was present.

The sequence of precipitate transformations that occurs during heat treatment, from the initial ssss to the equilibrium phase, can be expressed in terms of a precipitation sequence. For Al-Cu

alloy model with composition is Al-4 wt % Cu(1.7 atomic %), the precipitation sequence is [1] :-

$$ssss \Rightarrow GP \Rightarrow \theta'' \Rightarrow \theta' \Rightarrow \theta$$

2.3 Precipitation in Al-Mg-Si (6XXX) Alloys

This section deals with processes specific to aluminium-magnesium-silicon alloys. Precipitation phenomena is one of the most important issues to be studied in Al alloys since they are widely used to obtain high strength Al alloys in application. The main characteristic of the 6xxx alloys is the tremendous increase in hardness, due to the precipitation of Mg–Si metastable phases upon annealing at intermediate temperatures [3]. Heat treatment is used to promote the formation of needle-shaped precipitates from the supersaturated solid solution of Mg and Si in Al to achieve appreciable mechanical properties ([3],[5],[6]). The type of precipitate that gives rise to the maximum strength of alloys in the T6-condition is designated β", which has been found in electron diffraction studies to have a body centred monoclinic unit cell, a=15.34 Å, b=4.05 Å, c=6.83 Å and β =106° ([3],[7]) and a Mg_5Si_6 stoichiometry [8]. These precipitates are fine needles, ~30 nm long, lying parallel to the <001> directions of the matrix. When the alloy is over-aged, the hardening phase i.e. β" precipitates are dissolved and a number of coarser precipitates formed. In this condition, the alloy becomes softer [3]. It is generally accepted that the sequence of phases is of the form [3].

$$SSSS \Rightarrow \begin{pmatrix} clusters/co-clusters \\ of \\ Mg\ \&\ Si \end{pmatrix} \Rightarrow \begin{pmatrix} GP \\ Zones \end{pmatrix} \Rightarrow \beta'' \Rightarrow \beta'/\mathrm{B}/\cup \Rightarrow \beta(stable)$$

The types of precipitates found so far (mostly in over aged materials of these alloys) are shown in Table 2-1.

Table 2-1 Table summarizing the precipitates of the Al-Mg-Si alloy precipitation sequence and some of their properties.

Phase	**Formula**	**Unit Cell/ Crystal Structure**	**Morphology/ Typical Size**	**Reference**
GP	Probably $Mg_{5-x}Al_xSi_6$	Monoclinic	Spherical / Needles 1-2nm	[3],[15]
β"	Mg_5Si_6	Monoclinic a=15.16Å c=6.84Å	Needles/ 4 *x* 4 *x* 30nm	[3], [15]
β'	$Mg_{1.7}Si$	Hexagonal a=7.05Å Close packed hexagonal a=4.07Å	Ribbons/ several μm long	[3], [15]
β	Mg_2Si	Fcc (CaF_2 _type) a=6.39Å	Plates or Cubes/ Up to 10-20 μm	[3], [15]
B'	$\frac{Si}{Mg} \sim 1$	Hexagonal a=10.3Å	Ribbons/ Probably up to 1μm	[15]
U1	Si:Al:Mg=5:4:1	Hexagonal a=4.05Å	Rods/ ~100nm	[15]
U2	Si:Mg:Al=5:4:2	Orthorombic a=7.93Å	Rods	[[15]
Si		Cubic , fcc (diamond type) a=6.39Å	Thin Plates/ Up to 10-20 μm	[15]

2.4 Vacancies

The classical diffusion theory describes a mechanism involving nucleation of precipitates, growth and phase transformation which involves movement of substitutional atoms. In order for an atom to jump from one position in the lattice to another, an empty space, or vacancy is needed. Many precipitates nucleate at heterogeneous sites within the matrix. Of these, those which nucleate on dislocations are probably the most important in the context of accelerated aging metal matrix composites [2] .

In some cases, the nucleation of precipitates is aided by the presence of excess vacancies, which accelerate the kinetics of diffusional processes. A good example of this is provided by the formation Gunier-Preston zones (GPS) in Al-Cu [2]. Hence, the number of vacancies in the beginning of the ageing process increases the number of precipitates and at the same time reduces the growth rate. This in turn influences the macroscopic behaviour of alloys, with Hardness as a main parameter to describe it.

The equilibrium number of vacancies increases exponentially with rise in temperature, as shown in fig…..and, as a consequence, a knowledge of their behaviour is essential for understanding industrial processes occurring at elevated temperatures i.e. annealing, homogenization, precipitation, etc.[2]

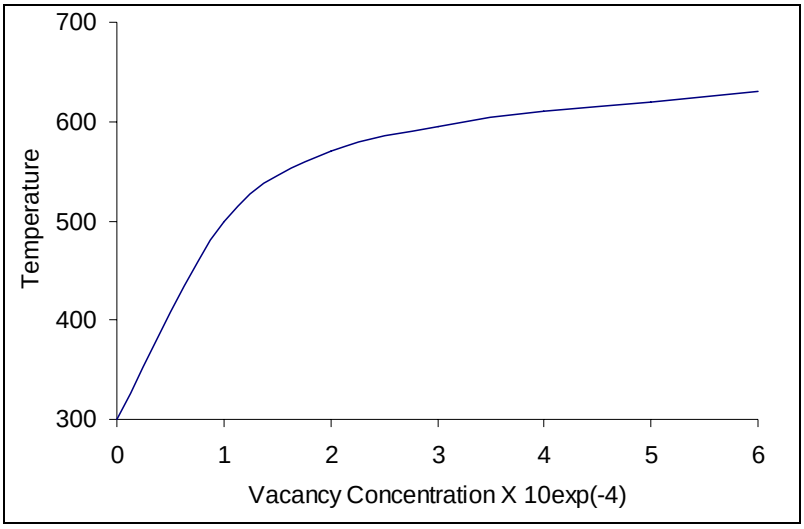

Figure 2-5 Equilibrium Concentration of Vacancies as a function of Temperature for Aluminium [2 p.130]

As the temperature is lowered to ageing temperature, concentration of vacancies should decrease in order to maintain equilibrium and to do this the vacancies must migrate to positions in the lattice ('Vacancy sinks') where they can be annihilated. Vacancy sinks include such places as grain boundaries, free surfaces and dislocations. The dislocations in the body of the grain or crystal are the most efficient 'sink' for vacancies[2]. When a metal is heated to homogenisation temperature the equilibrium concentration of vacancies increases and to produce this additional concentration the surfaces, grain boundaries and dislocations in the crystal reverse their role and act as vacancy sources and emit vacancies. However, below a certain temperature, the migration of vacancies will be too slow for equilibrium to be maintained, and at lower temperature a concentration of vacancies in excess of the equilibrium number will be retained in the lattice. Moreover, if cooling rate of the metal or alloy is particularly rapid, for example, in quenching, the vast majority of the vacancies which exist at high temperatures can be 'frozen-in' or 'quenched in'[2] . Given enough time, the excess vacancies relative to the equilibrium concentration will anneal out. There will be a tendency for vacancies to be attracted together into vacancy clusters, and some clusters collapse into dislocation loops, which can grow by absorbing more vacancies. The dislocations that are already present can also absorb vacancies by climbing. Hence, there are many ways in which

excess vacancies are able to provide heterogeneous nucleation sites [3]. Such vacancies are of considerable importance in governing the kinetics of many physical processes.

2.5 Structure of GP zones and β" in Al-Mg-Si alloys.

In section 2.2.5 page 17 we looked at the Solute clusters, the so called Guinier-Preston (G.P) zones which are initially formed during ageing process at low temperatures are found in a number of Al alloys such as Al-Mg-Si. Large number of studies has been carried out on the behaviour of G.P. zones in the process since G.P. zones significantly affect the properties of the alloys.

In his P.hD thesis, Calin Marioara investigated the ageing behaviour of a 6082 Al-Mg-Si alloy (this is almost similar to alloy A3 under the current investigation) at 150°C and his findings are summarised in Figure 2-6.

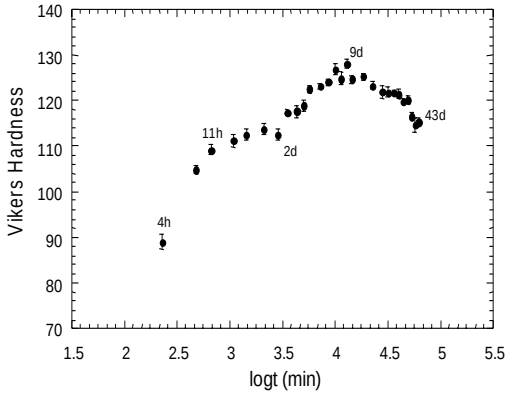

Figure 2-6 Vickers Hardness as a function of isothermal annealing time at 150 C of a 6082 Al-Mg-Si alloy with 0.6wt% Mg, 0.9wt% Si, 0.5wt% Mn and 0.2wt% Fe.[3]

He observed a double peak hardness curve one after 11 hours annealing time and the other after 9 days of annealing at 150°C. His investigations under high resolution microscopy(HRM)

showed that the first peak was due to the GP zones[2] and the second peak due to β" phase. Both of these phases are described below (see Figure 2-7). Note that the structure of the two phases is very similar and it is difficult to differentiate between them at low magnifications. In HREM images it is easy to differentiate between the GP zones and β" because the latter has the 'eye-structure' which is different from the super-lattice type structure of the former.

[2] From supersaturated solid solution (SSSS) atoms of Mg and Si aggregate into clusters that nucleate GP-zones,β" or other precipitate phases during the ageing heat treatment[3,12].

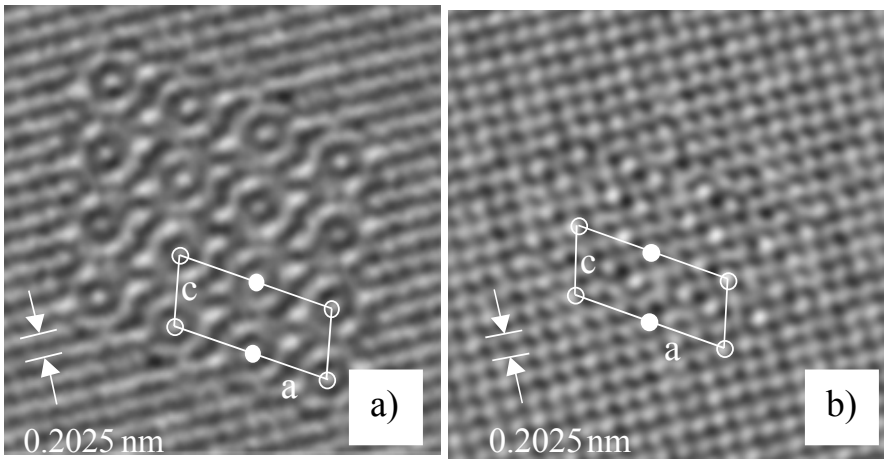

Figure 2-7 HREM images of (a) β" and (b) GP zone . In each image a unit cell is indicated

β" :-This is the main hardening phase. Slightly expanded super cell in Al. The Al FCC arrangement is broken Group: Monoclinic C2/m. Cell Parameters: a=15.16 Å ; b=4.05Å ; c=6.74Å ; γ=105.3° Composition: probably Mg_5Si_6 Unit cell packing (Va/Vc)=0.68. InCoherent interface [16].

Can be present in a very high number density since it nucleates from GP zones or probably directly from atomic clusters[18]. Seems incapable of nucleation/growth below 125°C[18]

GP-Zones: (Has been observed in Si rich alloys). This is a super cell in the Al matrix where Al atoms are being replaced by Mg and Si atoms. Have a very near structural relationship **β".** The Al FCC atomic arrangement is retained Group: Monoclinic C2/mCell Parameters: a=14.8 Å ; b=4.05 Å ; c=6.48Å ; γ=105.3° Composition: probably $Mg_{5-x}Al_xSi_6$ Unit cell packing (Va/Vc)=0.7. Coherent interface [17]. Are fully coherent and surrounded by a smaller strain field than **β".** Stabilised with a higher Si content.[3,18]

It has been known that Al-Mg-Si alloys containing Si to excess (excess Si alloys) are higher strength than balanced Al-Mg-Si alloys (balanced alloys) and it is believed the refinement of the precipitates leads to that phenomena[13]. The excess Si in the Al matrix forms clusters (containing Si, Mg or vacancies) and they act as the nucleation sites for fine precipitates [13]. In the present investigation, both Si-rich and Mg-rich alloys are considered.

2.6 Hardening Mechanisms

In this section, we look at how these precipitates strengthen the alloy by inhibiting dislocation mobility. To increase the strength of metals in general, it is necessary to impede the movement of dislocations. This is because Plastic deformation by metals is caused by the motion of dislocations. Impeding this motion therefore results in alloy strengthening.

The strengthening which results from heat treatment depends on the nature of the precipitates formed.

Three mechanisms can be identified:-

2.6.1 Coherency strain hardening

This is due to the resistance to dislocation motion provided by coherency strain fields. The precipitation of particles having a slight misfit in the matrix gives rise to stress fields, which hinder the movement of gliding dislocations [2].

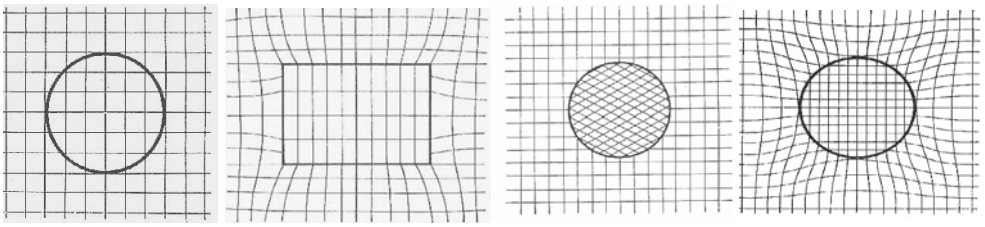

a)Fully Coherent b) partly coherent c)Non-coherent d)Fully coherent with small misfit

Figure 2-8 Schematic representation of various precipitate-matrix interfaces [21].

The thin lines in Figure 2-8 indicate atomic planes while thick lines indicate precipitate-matrix interfaces. (a) Shows a fully coherent interface with a perfect match between the atomic planes of the precipitate and host matrix. (c) Shows the non-coherent interface with no match between atomic planes. (d) Coherent interface subject to misfit strains as the lattice parameters differ.

In solid solution strengthening, the substitution of the solute atoms for Al ones distorts crystal lattice, hinders dislocation mobility and hence strengthens the alloy (see also section 2.1.1 page 11). In order to be effective solid solution strengtheners alloy additions must satisfy 2 criteria:-

- high room temperature solid solubility and
- atomic misfit to create local compressive or tensile strains.

2.6.2 Chemical hardening

Is due to the increase in applied stress required to shear/cut a coherent precipitate.

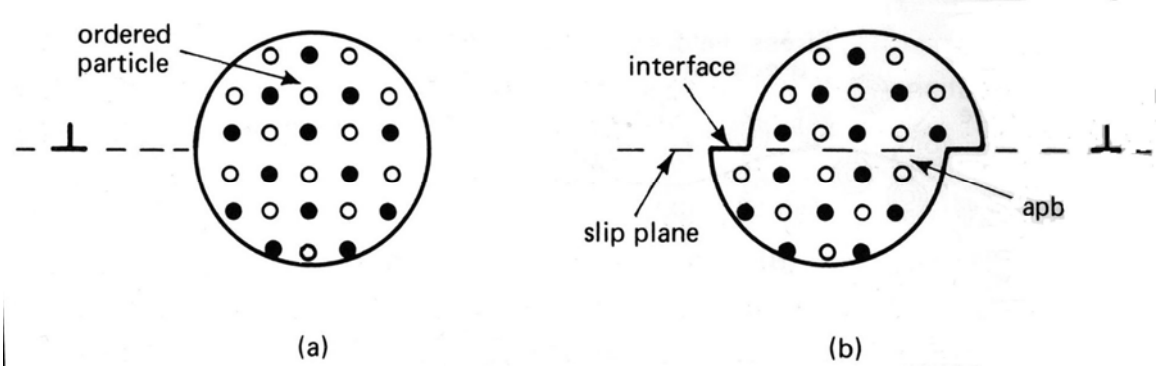

Figure 2-9 Ordered particle (a) cut by dislocations in (b) to produce new interface and apb [2]

2.6.3 Dispersion Hardening

At higher ageing times and/or temperatures, precipitates become incoherent and dislocations are no longer able to cut through them. Instead, they must by-pass the precipitate by one of a number of possible mechanisms. These include bowing, climb and cross-slip.One important

feature of dispersion hardened materials is the diffuse (non-localised) nature of slip. This has important consequences in terms of mechanical properties.

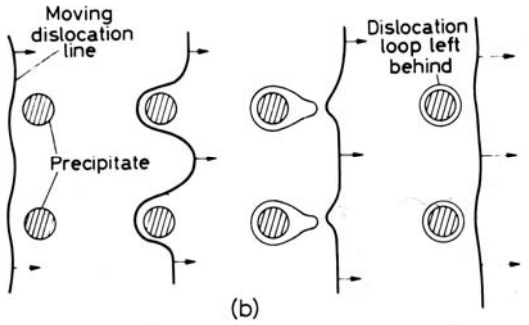

Figure 2-10 Schematic representation of a dislocation passing between widely spaced precipitates (Orowan looping) [2]

2.6.4 ***The ageing Curve for Aluminium alloys***

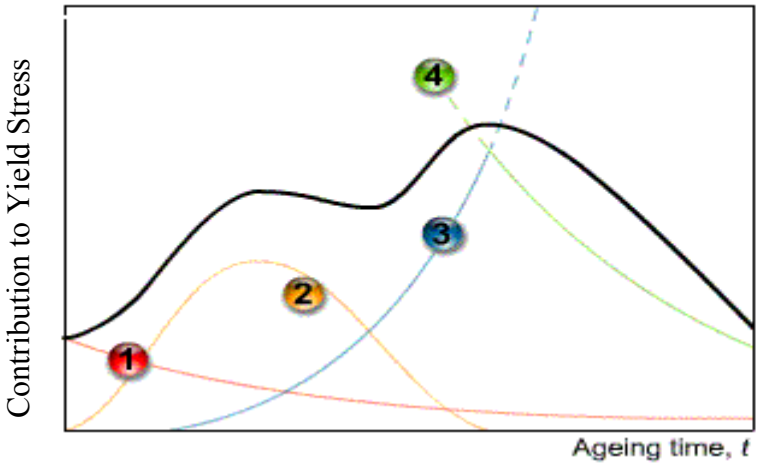

Figure 2-11 Contribution from Solute hardening, chemical hardening, dispersion hardening and coherency strain hardening to Yield Stressl [10].

*Solute Hardening (*represented by curve 1*)*:-As GP zones and other precipitates are formed, it follows that there is a corresponding reduction of solute in the phase. The contribution of solute hardening to the overall alloy strength therefore diminishes during ageing. It will reach a stable value when the phase reaches its equilibrium composition.

Coherency Strain Hardening (curve 2) :- As the GP zones nucleate and grow, there is an increase in the level of coherency strain hardening. This reaches a maximum when the average zone separation is about equal to the limiting radius of dislocation curvature. Coherency strain hardening is due to the resistance to dislocation motion provided by coherency strain fields [12].

Chemical Hardening (curve 3*)*:- The increase in stress required to force a dislocation through a coherent zone/precipitate is termed chemical hardening As the number and size of coherent precipitates increases, the role of chemical hardening becomes greater. However, as the precipitates reach a certain size, coherency starts to break down, and they can no longer be cut by dislocations. Chemical hardening is due to the increase in applied stress required to cut/shear a coherent precipitate [12].

Dispersion Hardening (curve 4):- As new incoherent precipitates start to form, dispersion hardening becomes the dominant strengthening mechanism. At longer ageing times, these precipitates tend to coarsen, and the strengthening effect decreases. Note that the transition between chemical and dispersion hardening is rarely abrupt- the two mechanisms can operate within the same alloy. At higher ageing times and/or temperatures, precipitates become incoherent and dislocations are no longer able to cut through them.Instead, they must by-pass the precipitate by one of a number of possible mechanisms. These include bowing, climb and cross-slip. Dispersion hardening is due to the increase in applied stress required to by-pass an incoherent precipitate or particle.

Combined Ageing Curve:- The overall ageing curve is based on the 4 component curves. Curves 1, 2 and 3 are roughly additive. Curves 3 and 4 represent competing mechanisms, so the overall strength will be a weighted average of the two.

2.7 Tensile properties

To determine the load-carrying ability and the amount of deformation before fracture, a sample of material is commonly tested by a Tensile Test. This test consists of applying a gradually increasing force of tension at one end of a sample length of the material. The other end is anchored in a rigid support so that the sample is slowly pulled apart. The testing

machine is equipped with a device to indicate, and possibly record, the magnitude of the force throughout the test. Simultaneous measurements are made of the increasing length of a selected portion at the middle of the specimen, called the gage length. The measurements of both load and elongation are ordinarily discontinued shortly after plastic deformation begins; however, the maximum load reached is always recorded. The tensile test supplies three descriptive facts about a material. These are;- (a) the stress at which observable plastic deformation or "yielding" begins; (b) the ultimate tensile strength or maximum intensity of load that can be carried in tension; and (c) the percent elongation. Young's Modulus (Elastic Modulus) is the ratio of stress to strain, or the gradient of the stress-strain graph. It is measured using the following equation 2-3:

2.8 Engineering Stress and Engineering Strain

Aluminium is ductile and has a low melting point and density. In a molten condition it can be processed in a number of ways. Its ductility allows products of aluminium to be basically formed close to the end of the product's design. Consider a uniform cylindrical bar, which is subjected to en axial tensile load (Figure 2-12).

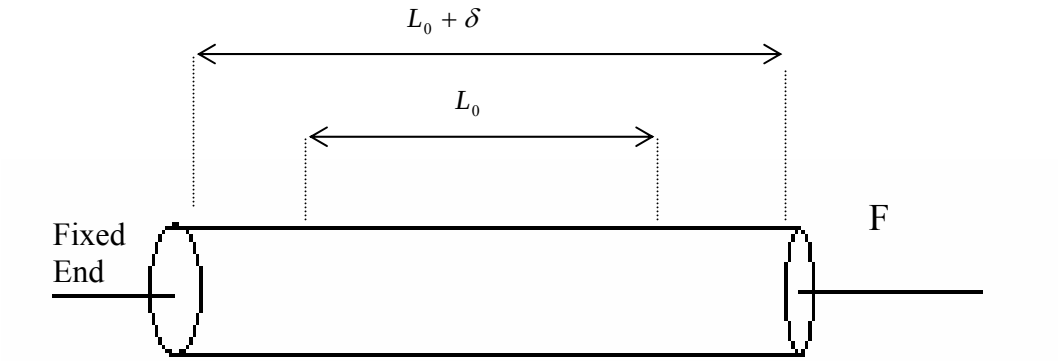

Figure 2-12 Cylindrical bar subjected to axial load

A load F is applied to one end of the bar and the gauge length undergoes a slight increase in length and decrease in diameter. The distance between the gauge marks has increased by amount δ, called the deformation.

The average engineering linear strain, e is the ratio of the change in length to the original length.

$$e = \frac{\delta}{L_0} = \frac{\Delta L}{L_0} = \frac{L - L_0}{L_0} \qquad (2\text{-}1)$$

Average engineering stress is obtained by dividing the load by the original area, Ao, of the cross section of the specimen.

$$Stress, \sigma = \frac{Load}{Cross - \text{sec}tional} = \frac{F}{A_0} \qquad (2\text{-}2)$$

Below the elastic limit, Hooke's law can be considered valid, so that the average stress is proportional to the average strain.

$$\frac{\sigma}{e} = E \qquad (2\text{-}3)$$

Young's Modulus (sometimes referred to as Modulus of Elasticity, meaning "measure" of elasticity) is an extremely important characteristic of a material. The constant E in equation (2-3) is the modulus of elasticity or Young's modulus. E is a measure of the stiffness of the material and is determined by the binding forces between atoms.

The shape and magnitude of the engineering stress vs engineering strain curve of a metal will depend on its composition, heat treatment, prior history of plastic deformation, and the strain rate, temperature and the state of stress imposed during the testing.[11]

The parameters, which are used to describe the engineering stress vs engineering strain curve of a metal are strength (i.e. tensile strength and Yield strength) and ductility (i.e. percent elongation and reduction of area).

2.8.1 Tensile strength

The tensile strength or ultimate tensile strength (UTS) is the maximum load divided by the original cross sectional area of the specimen.

$$UTS = \frac{F_{\max}}{A_0} \qquad (2\text{-}4)$$

- UTS is used for the purposes of specifications and for quality control of a product.
- For brittle materials, UTS is a valid criteria for design.

For ductile metals, the tensile strength should be regarded as a measure of the maximum load, which a metal can with stand under very restrictive conditions of uniaxial loading.

Measures of ductility

Measures of ductility are of interest in three ways

- To indicate the extent to which a metal can be deformed without fracture in metalworking operations such as rolling and extrusion.
- To indicate to the designer in a general way, the ability of the metal to flow plastically before fracture. A high ductility indicates that the material is forgiving and likely to deform locally without fracture should the designer err in the stress calculation or the prediction of severe loads.
- To serve as an indicator of changes in impurity level or processing conditions. Ductility measures may be specified to asses material quality even though no direct relationship exists between the ductility measurement an the performance in service.

The conventional measures of ductility that are obtained from the tension test are the engineering strain at fracture e_f (usually called elongation) and the reduction area at fracture q. Both of these are obtained after fracture by putting the specimen back together and taking measurement of L_f and A_f .

$$e_f = \frac{L_f - L_0}{L_0} \qquad (2\text{-}5)$$

$$Q = \frac{A_0 - A_f}{A_0} \qquad (2\text{-}6)$$

Both elongation and reduction of area are usually expressed as a percentage. Elongation depends on gauge length L_0, over which the measurement was taken. The smaller the gauge length the greater will be the contribution to the overall elongation from the necked region and the higher will be the value of e_f. Therefore when reporting value of percentage elongation, the gauge length L_0 must be given.

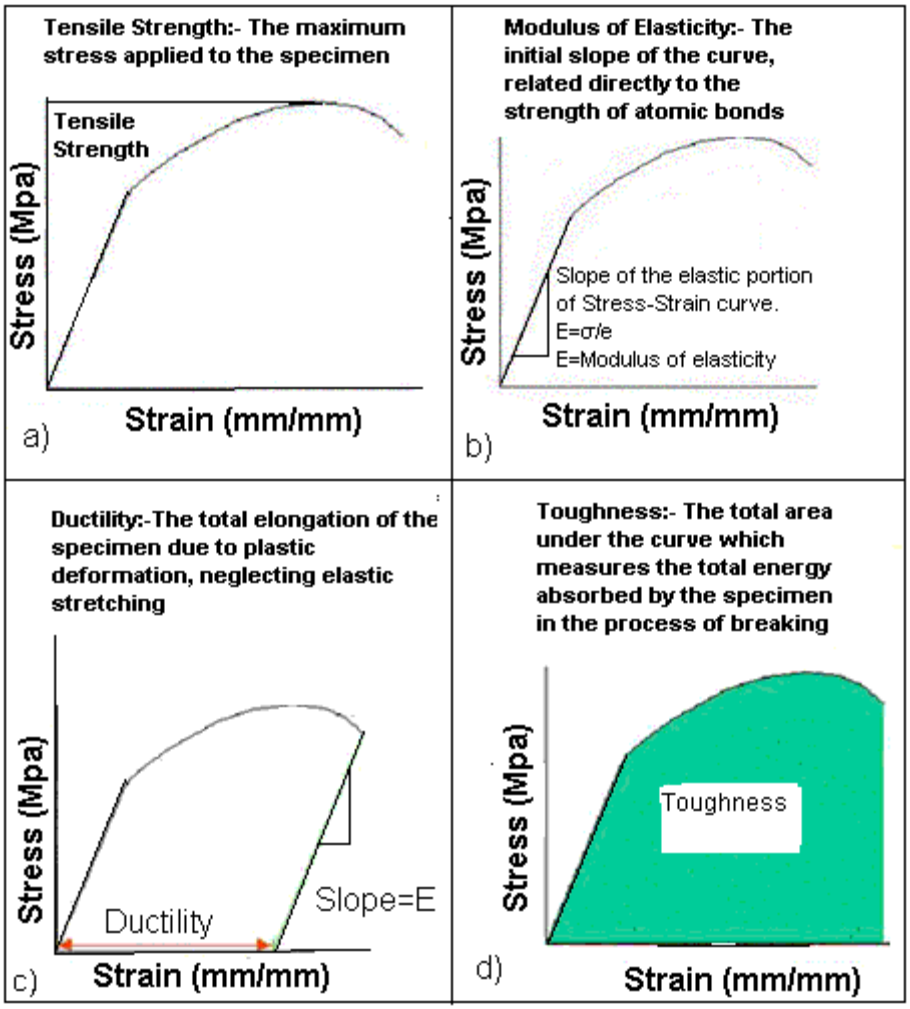

Figure 2-13 Stress – Strain curves illustrating (a) Tensile Strength (b) Modulus of elasticity (c) ductility and (d) toughness

Initially the material deforms elastically. Above the yield stress, the material starts to deform plastically. Dislocations multiply rapidly and their strain fields interact. If the load is removed just after the yield stress, the material will show some permanent deformation. At the point of Tensile strength region, strain localises so that a "neck" starts to form on the test piece. Final structure occurs when the reduced cross-section can no longer support the load.

Ductility: The total elongation of the specimen due to plastic deformation, neglecting the elastic stretching.

Toughness: The total area under the curve, which indicates the energy absorbed by the specimen in the process of breaking.

2.8.2 Elastic limit:

The largest value of the stress for which the material will return to its original length after the stress is removed is called the elastic limit. If the material is stressed beyond this limit, then it behaves inelastically and will have permanent deformation .

2.9 Grains

There are 4 main casting variables that influence mechanical properties of cast alloys:- *Porosity, Presence of second phase, Dendrite spacing and Grain size* [1]. Reducing the grain size increases the alloy strength according to the Hall-Petch relationship

$$\sigma = \sigma_0 + k/\sqrt{d} \qquad (2\text{-}7)$$

σ=stress and σ_0 = Yield Stress k=a means of the difficulty required to unlock or generate dislocations in the neighbouring grain.

i.e. a linear relationship between flow stress and the reciprocal of the square root grain diameters. Equation (2-7) shows that strength is directly proportional to the reciprocal of the square root of the grain diameter.

The strengthening product by the microstructure results from blockage of dislocation motion by the interfaces of the microstructure. If a source within a given grain is feeding dislocations into a grain boundary, the dislocation motion will eventually become blocked at that boundary. Further motion then requires generation of new dislocations in the neighbouring grain by means of the local stress field generated by the blocked dislocations in the parent grain.

2.10 Electrical Conductivity

Electrical conductivity test is very ueful in :-

- Investigation of phase transformation ●Substructure defects and
- Concentration dependencies in metals and alloys.

Conductivity is proportional to the concentration of carriers, and to their mobility. The basic equation, which is just a form of Ohm's law, may be written as :-

$$J = \sigma E \qquad (2\text{-}8)$$

Where J is the current density (Am^{-2}) and σ is the conductivity ($\Omega^{-1}m^{-1}$) and E is the electrical field (Vm^{-1}). The reciprocal of conductivity is the resistivity ϱ (Ωm). Only electrons or ions can act as carriers of electric charge. Because electrons are much more mobile than ions, metals have greater conductivities because they have free electrons. Impurities or alloying elements tend to cause a sharp reduction in conductivity (rise in ϱ). This is due to scattering of electrons by atomic scale disturbances to the potential field of the lattice. The increased dislocation density caused by the annealing treatments can raise the in situ resistivity of the matrix [4]. In summary, the electrical resistance of a metal is found to be due to interactions of the valence electrons with

- The thermal vibrations of the ions
- Impurities and
- Imperfections in the crystal

Conductivity is often measured by an Eddy current technique.

2.11 Eddy Current

Conductivity is often measured by an eddy current technique. A brief introduction to Eddy current is given. When an AC current flows in a coil in close proximity to a conducting surface the magnetic field of the coil will induce circulating (eddy) currents in that surface. The magnitude and phase of the eddy currents will affect the loading on the coil and thus its impedance.

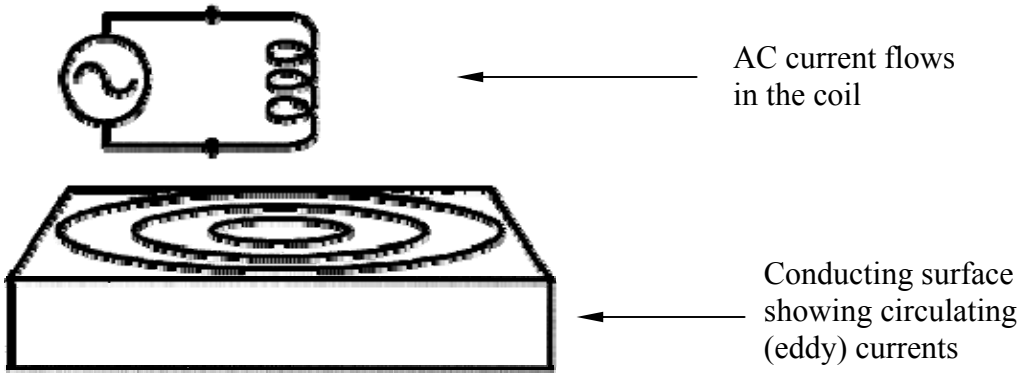

Figure 2-14 Simple coil above a metal surface. Demonstration of the basics of eddy current testing

As an example, assume that there is a deep crack in the surface immediately underneath the coil. This will interrupt or reduce the eddy current flow, thus decreasing the loading on the coil and increasing its effective impedance. This is the basis of eddy current testing, by monitoring the voltage across the coil in such an arrangement we can detect changes in the material of interest. Note that cracks must interrupt the surface eddy current flow to be detected. Cracks lying parallel to the current path will not cause any significant interruption and may not be detected. The conductivity of a material has a very direct effect on the eddy current flow: the greater the conductivity of a material the greater the flow of eddy currents on the surface. Conductivity is often measured by an eddy current technique, and inferences can then be drawn about the different factors affecting conductivity, such as material composition, heat treatment, work hardening etc.

2.12 Transmission Electron Microscopy

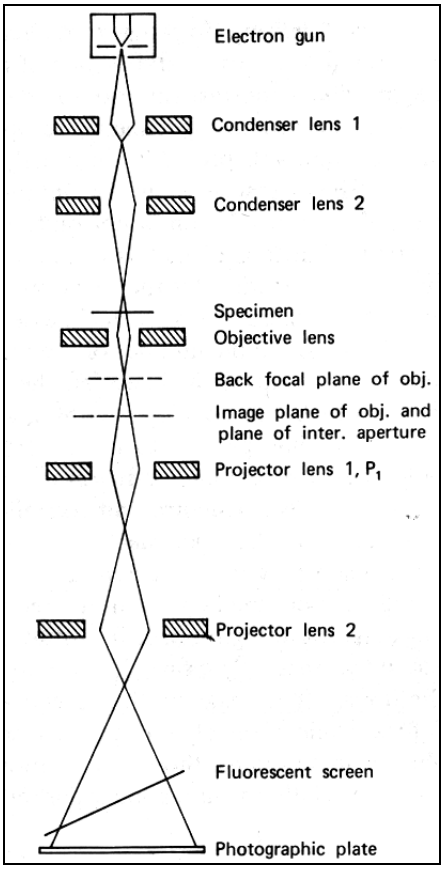

Figure 2-15 Schematic view of electron optics in the TEM column [1]

The Transmission Electron Microscope (TEM) allows the user to determine the internal structure of materials. Specimens for TEM must be specially prepared to thickness, which allow electrons to transmit through the sample, much like light is transmitted through materials in conventional optical microscopy. Because the wavelength of electrons is much smaller than that of light, the optimal resolution attainable for TEM images is many orders of magnitude better than that from a light microscope. For example, the wavelength of green light is ~550nm and the resolution of a good light microscope is ~300nm[3]. In contrast, a 100keV electron has a wavelength of 0.004nm, which is much smaller than the diameter of an atom. Thus, TEMs can reveal the finest details of internal structure - in some cases as small as

individual atoms. Phase determination as well as defect and precipitate orientation are typical outcomes of conventional TEM experiments. Microstructural characterization of materials, including unit cell periodicities, can be readily determined using various combinations of imaging and electron diffraction techniques. Images obtained from a TEM are two-dimensional sections of the material under study, but applications, which require three-dimensional reconstructions, can be, accommodate by these techniques.

1. The electron gun, produces a stream of monochromatic electrons.

2. This stream is focused to a small, thin, coherent beam by the use of condenser lenses 1 and 2. The first lens(usually controlled by the "spot size knob") largely determines the "spot size"; the general size range of the final spot that strikes the sample. The second lens(usually controlled by the "intensity or brightness knob" actually changes the size of the spot on the sample; changing it from a wide dispersed spot to a pinpoint beam. Instead of optical lenses, the TEM utilises magnetic lenses[3].

3. The beam is restricted by the condenser aperture (usually user selectable), knocking out high angle electrons (those far from the optic axis, the dotted line down the center

The beam strikes the specimen and parts of it are transmitted

[3] Circular electro-magnets capable of projecting a precise circular magnetic field in a specified region. The field acts like an optical lens, having the same attributes (focal length, angle of divergence..etc) and errors (Spherical aberration, chromatic aberration ..etc). They are used to focus and steer electrons in the TEM.

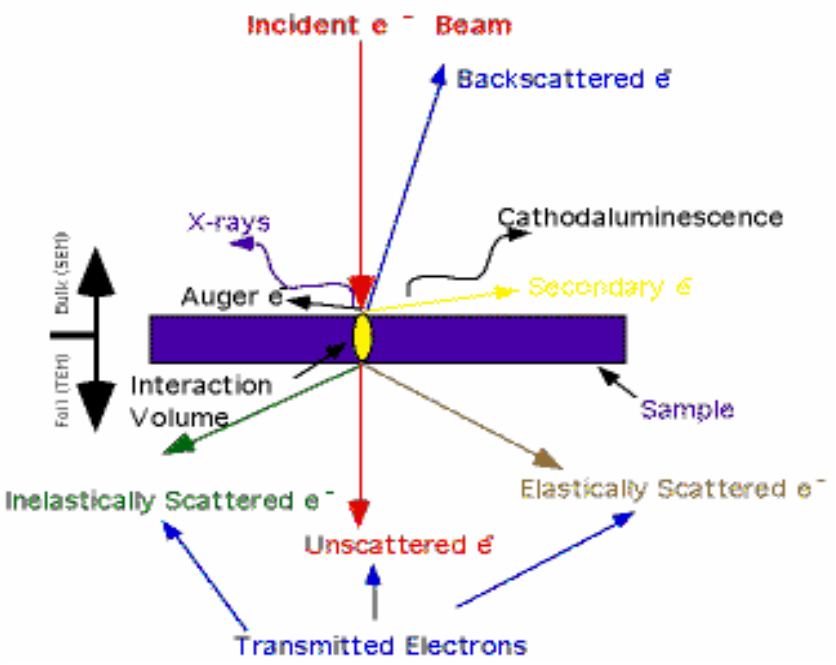

Figure 2-16 Electron beam and Specimen interaction. The beam strikes the specimen and parts of it are transmitted [1]

4. This transmitted portion is focused by the objective lens into an image

5. Optional Objective and Selected Area metal apertures can restrict the beam; the Objective aperture enhancing contrast by blocking out high-angle diffracted electrons, the Selected Area aperture enabling the user to examine the periodic diffraction of electrons by ordered arrangements of atoms in the sample

6. The image is passed down the column through the intermediate and projector lenses, being enlarged all the way

7. The image strikes the phosphor image screen and light is generated, allowing the user to see the image. The darker areas of the image represent those areas of the sample that fewer electrons were transmitted through (they are thicker or denser). The lighter areas of the image represent those areas of the sample that more electrons were transmitted through (they are thinner or less dense)

2.12.1 Electron Diffraction

Electrons entering a material interact with the constituent atoms through electrostatic forces and are scattered. Figure 2-17 below indicates the reflection of a plane wave incident on atomic planes.

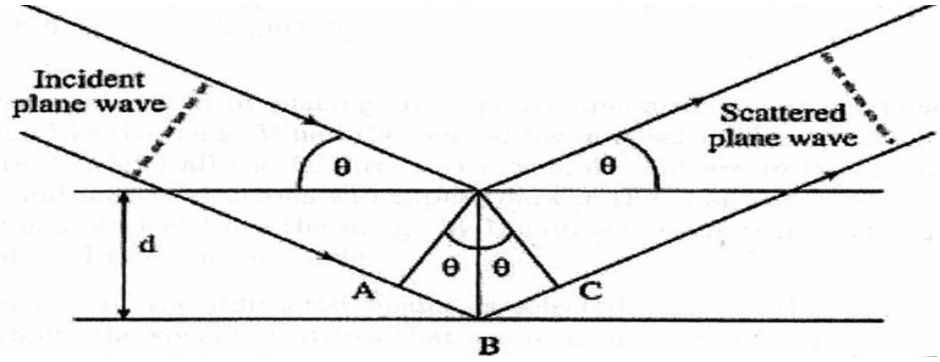

Figure 2-17 The Bragg description of diffraction in terms of the scattering of a plane wave of wavelength λ incident at an angle θ to atomic planes of spacing d [9]

When the scattered electrons recombine, they may interfere either constructively or destructively. To interfere constructively the electron wave must scatter through the Bragg angle θ_B, given by the wavelength λ and the distance d between the two planes on which the beams scatter[9].

$$N\lambda = 2d\sin\theta_B \qquad (2\text{-}8)$$

The electron beam passing through the sample is diffracted if any set of (hkl) planes satisfy the Bragg equation (2-8)[9]

2.12.2 Diffraction Patterns, Bright Field and Dark Field

A magnified image of the specimen is produced by the objective lens in the image plane or a diffraction pattern in the back focal plane . By changing the focal length of the projector lenses, one of the two images is visualized. The microscope thus can work in image mode, or in diffraction mode.

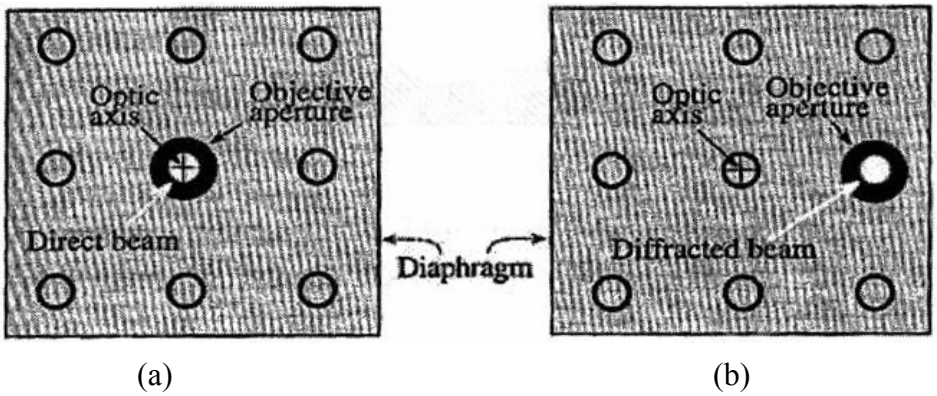

Figure 2-18 Ray diagram illustrating the making of a) a bright field and b) a dark field image [9]

Contrast is created by placing an objective aperture in the back focal plane of the objective lens. When the central beam is selected to form the image Fig…a) all the features in the sample that are in Bragg condition and scatter electrons will appear dark in the image because these electrons are blocked from the image by the objective aperture. This is called bright field(BF) image mode.

When one of the diffracted beams is selected to form the image in Figure 2-18 (b) the specific features that are in Bragg condition and scatter the electrons selected by the aperture will appear bright in the image. This is called dark field (DF) image mode.

The spots in the diffraction pattern represent the reflections, which have interfered constructively upon the Bragg angle. The direct (unscattered) beam is defined as the 000 reflection. Each reflection from a diffracted beam is given different hkl indices corresponding to the hkl planes in the diffraction pattern..

2.12.3 Electron Energy Loss Spectroscopy (EELS)

The specimen thickness, which depends on the mean free path λ, for inelastic scattering is measured using a Gatan model 666 parallel-detection electron energy loss spectrometer mounted on the Philips CM 30 Transmission Electron microscope, equipped with a LaB6 filament. EELS is very useful in measuring the thickness of a TEM specimen. It entails analysing the energy distribution of initial monoenergetic electrons after having interacted with a TEM specimen

The electron beam transmitted through the specimen is directed into a high resolution electron spectrometer separating the electrons according to their kinetic energy. These different energies produce an electron energy-loss spectrum indicating the scattered intensity as a function of the decrease in energy of the electron.

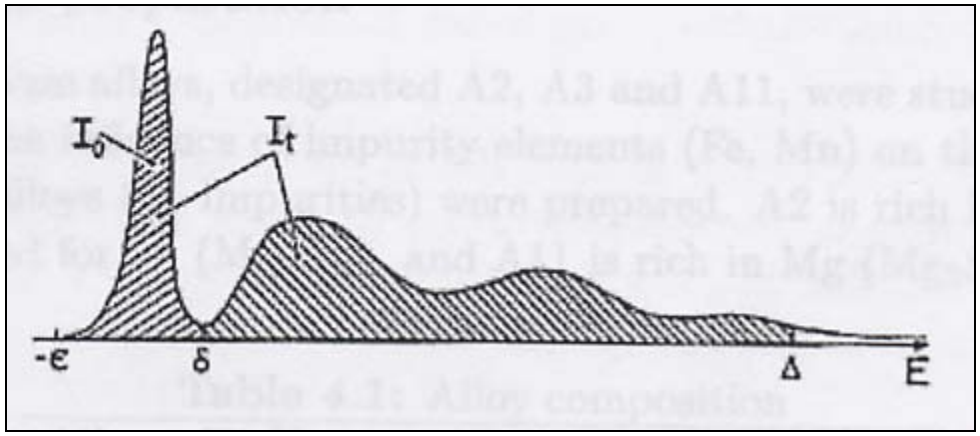

Figure 2-19 EELS spectrum. The integrals and energies involved when measuring specimen thickness [9]

A schematic view of an EELS spectrum with its corresponding energies is shown in Figure 2-19. The zero loss peak represents the electrons transmitted without any measurable energy loss, including the unscattered electrons. The other peaks represent electrons that have suffered various amounts of energy loss after interacting with the specimen.

In order to measure the thickness of a specimen, an energy-loss spectrum is recorded and the area I0 under the zero-loss peak is compared to the total area It under the whole spectrum.

The energies ε, δ and Δ define the limits of integration. ε, gives the lower limit of the zero-loss region, δ gives the first intensity minimum, while Δ is the upper limit of integration where further contributions to It are insignificant.

The relative specimen thickness t / λ is given by

$$\frac{t}{\lambda} = In\left(\frac{I_t}{I_0}\right) \qquad (2\text{-}9)$$

Where λ is the total mean free path for all Inelastic scattering. The mean free path gives a measure of the scattering intensity from each atom [9] and depends on the high tension used for exciting the electrons, and on the material studied. In this investigation, a high tension of 150kV was used, corresponding to equation

$$\lambda_{150Kv}^{Al} = 111nm \qquad (2\text{-}10)$$

for pure aluminium

This value was used as an approximation for the 2 alloys under investigation the alloying elements not withstanding.

3 Chapter 3 EXPERIMENTAL TECHNIQUES

This chapter presents the experimental apparatus used and procedure followed in performing the investigation. The present work has been concentrated on two different AL-Mg-Si alloys one of which is near 6082 and β" optimized.

3.1.1 Sample Preparation

Two industrially important Aluminium alloys, in form of extrusion bars and designated A3 and A12 were obtained from Hydro Aluminium Industry, Sundalsøra, for this investigation. All the alloys were produced according to standard industrial practice. The composition of the alloys is shown in Table 3-1

Table 3-1 Composition of the investigated alloys

Alloy	**Solute Content**		**Total (Si+Mg)at%**	**Solute Ratio (Si/Mg)**
	wt%	**At%**		
A3	0.75Si 0.52Mg	0.721Si 0.577Mg	0.721Si 0.577Mg	1.25, Si-rich Near 6082 β"-optimized
A12	0.59Si 0.65Mg	0.57Si 0.72Mg	0.57Si 0.72Mg	0.8 Mg-rich

Prior History of the Alloys

Each alloy had weighed 4kg before casting and was homogenized at 570 °C for 2 hours before it was extruded at ~400 °C to 500 °C, quenched and stored at room temperature for several months.

The extruded bars were cut to pieces of dimensions 25mmx25mmx2mm, as shown in

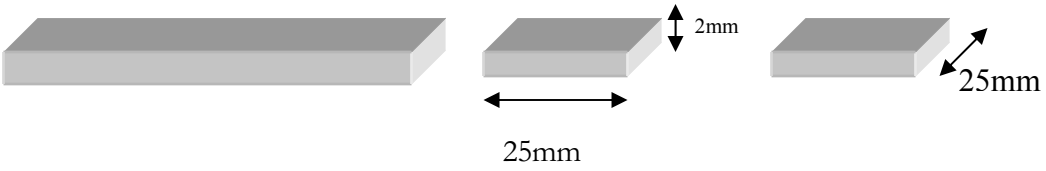

Figure 3-1 Cutting of alloy specimens

The cut samples were ground on SiC paper at 800 and divided into two equal groups i.e. Group (i) and Group (ii). These were studied under two different solution heat treatment temperature conditions but same ageing temperature condition. Pure alloys (which do not contain impurity elements (dispersoids2) such as Fe, Mn) were used in this experiment in order to minimize the influence of dispersoids on their microstructure

3.2 Heat Treatment

The Group (i) samples, A3 and A12, were solution heat treated in a salt bath at 570°C for 2 hours, then quenched in water and held at room temperature for 4 hours. Thereafter, the samples were annealed in an oil bath at 175°C for a time varying from 30minutes to 200hours and subsequently quenched in water.

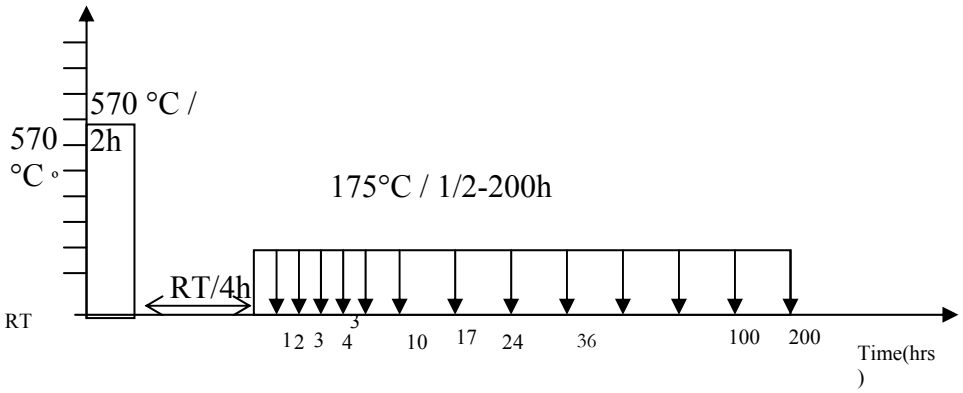

Figure 3-2 Heat treatment and hardness measurement procedures for Group (i) Samples

Group (ii) samples of A3 and A12 were solution heat treated in a salt bath at 520°C for 10minutes, then quenched in water and held at room temperature for 4 hours before they were annealed/aged in an oil bath at 175°C for a time varying from 30minutes to 200hours.

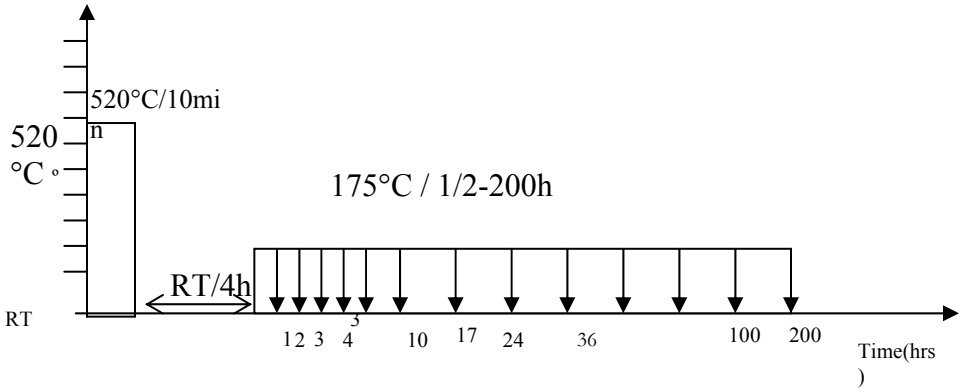

Figure 3-3 Heat treatment and hardness measurement procedures for Group (ii) Samples

These heat treatments are described in Table 3-2. Sample labelling has been done using three numbers Ax / xxx / xxh. The first number, AX, refers to the alloy type (i.e. A3 0r A12) the second, xxx, stands for solution heat temperature (i.e. 570°C for 2hours or 520°C for 10 minutes). The third number, xxh, indicates the annealing time at 175°C, while the symbol h stands for hours. It is important to remember that all samples were stored at room temperature for 4 hours prior to being aged.

Table 3-2 Heat treatment and sample description

Alloy	Solution Heat Temp.	Ageing Temp.	Annealing Time	Sample description
A3	570°C for 2hrs and 4hrs RT	175°C	30min , 1hr 2hrs , 3hrs 4.5hrs, 6hrs 10hrs, 17hrs 24hrs, 36hrs 100hrs, 200hrs	A3 /570/0.5h, A3 /570/1h A3 /570/2h, A3 /570/3h A3 /570/4.5h, A3 /570/6h A3 /570/10h, A3 /570/17h A3 /570/24h, A3 /570/36h A3 /570/100h, A3/570/200h
A12	570°C for 2hrs and 4hrs RT	175°C	30min, 1hr 2hrs, 3hrs 4.5hrs, 6hrs 10hrs, 17hrs 24hrs, 36hrs 100hrs, 200hrs	A12 /570/0.5h, A12/570/1h A12 /570/2h, A12 /570/3h A12 /570/4.5h, A12/570/6h A12 /570/10h, A12/570/17h A12 /570/24h, A12/570/36h A12/570/100h,A12/570/200h
A3	520°C for 10mins and 4hrs RT	175°C	30min, 1hr 2hrs, 3hrs 4.5hrs, 6hours 10hrs, 17hrs 24hrs, 36hrs 100hrs, 200hrs	A3 /520/0.5h, A3 /520/1h A3 /520/2h, A3 /520/3h A3 /520/4.5h, A3 /520/6h A3 /520/10h, A3 /520/17h A3 /520/24h, A3 /520/36h A3 /520/100h, A3/520/200h
A12	520°C for 10mins and 4hrs RT	175°C	30min, 1hr 2hrs, 3hrs 4.5hrs, 6hrs 10hrs, 17hrs 24hrs, 36hrs 100hrs, 200hrs	A12 /520/0.5h, A12 /520/1h A12 /520/2h, A12 /520/3h A12 /520/4.5h, A12 /520/6h A12 /520/10h, A12/520/17h A12 /520/24h, A12/520/36h A12/520/100h,A12/520/200h

3.3 Grain size specimen preparation and measurement

Three important steps were followed in preparing samples for grain size measurements: - Mechanical grinding (to produce a plane surface with minimal damage that can be removed easily during polishing), electropolishing (to etch away any damaged surface) and anodising (to reveal grain structure). Each specimen was ground on SiC – paper to a grid size of 4000 followed by polishing on a MD MOL cloth with 3μm diamond spray and on MD Nap cloth with 1 μm diamond spray. They were then electropolished on a Struers Lectropol-5 instrument at a voltage of 21V for 4 seconds at a temperature 13°C and a flow rate of 3 in a solution (electrolyte) of 7.8% perchloric acid, 10% butylgycol, 12% distilled water and 70%ethanonal. Finally, the samples were anodised in 5% HBF4 aqueous solution (Barkers reagent) at 20V, current of 1A for 90 seconds at 18°C and a flow rate of 4 to reveal the grain structure.

Grain Size measurements were done with a light microscope[4] by determining the number of grains (or grain boundaries) that intersect a given length of a random line as summarized in Figure 3-4. The grain size of alloys A3 and A12 were measured before and after being deformed by the tensile test and the mean results are summarised in Table 4-1 i.e. (i) in the as extruded form, (ii) after solution heat treatment as outlined in section 3.2 page 45 prior to (i) 3 hours and (ii) 17 hours ageing in an oil bath at 175°C and (b) after tensile testing (deformation) respectively.

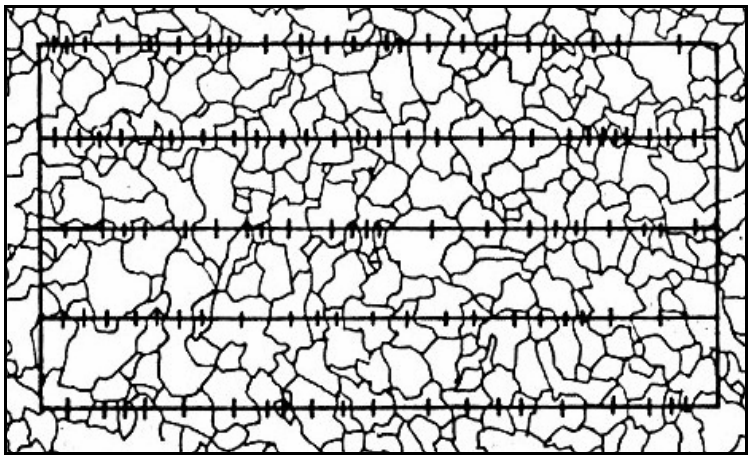

Figure 3-4 Measurement of grain diameter by intercept method

[4] Compared to other techniques like TEM, the light optical microscope has a low resolution, but provides a large field of view

In this investigation, the mean intercept length of random test lines was employed as a measure of grain size. Dividing the total length of test line by the number of grains traversed made this determination. The measurements of the grain size were done by linear intercept method

3.4 Hardness Measurements

Hardness measurements were used as an indicator of mechanical response to aging. The sample hardness was measured using a Matsuzawa DVK- 1S to perform Vickers Hardness Test. The load used was 1kgf, the loading speed 100um/s, and the pressing time 15 seconds. A small square-based pyramidal diamond indenter having included face angles of 136° (see Figure 3-5) was forced into the sample surface. The resulting impression, diagonals d_1 and d_2, were measured in a light microscope, and a corresponding unitless hardness number, HV was automatically computed from the equation (3-1).

$$HV = \frac{2P\sin\left(\alpha/2\right)}{d^2} = \frac{2P\sin\left(136^0/2\right)}{d^2} = 1.8544\frac{P}{d^2} \qquad (3\text{-}1)$$

Where

P= load, kgf , d =mean diagonal of impression ,mm, and, α = face angle diamond=136°

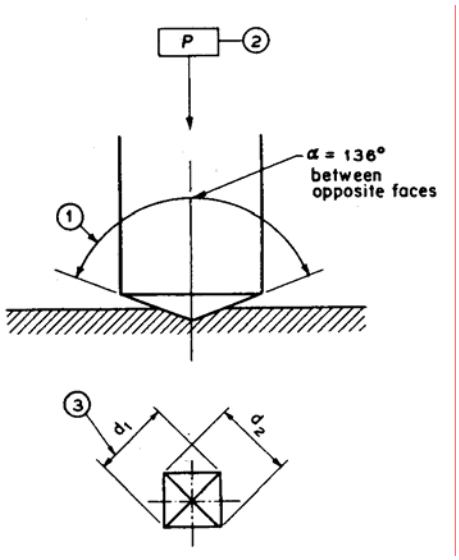

Figure 3-5 Vickers Hardness Test

The sample hardness was measured immediately after solution heat treatment as described in page 45, and then again when taken out of the ageing salt bath, as illustrated in Figure 3-2 and Figure 3-3. Surface grinding was done to remove the coating on the surface of the specimen produced by the heat treatment, so that the impressions were more easily visible for ease of correct measurement. 12 specimens were used to measure hardness for each alloy. To obtain the hardness numbers for each annealing time, the measurements were at 10 to 15 randomly chosen locations. A different sample was used for each data point. 10-15 indentations made the basis for one data point. The changes in hardness with annealing time are summarised in Figure 4-12 for each alloy and for each solution heat treatment.

3.5 Electrical conductivity

Electrical Conductivity of all samples was measured by an eddy current technique, and inferences were then drawn about the different factors affecting conductivity, such as material composition, heat treatment, solute elements etc. All conductivity measurements of the samples were done using an instrument called SIGMATEST D model 2.068, a microprocessor-controlled eddy-current instrument. For measuring the conductivity of the samples, the following were required: - a probe, a probe cable and a calibration standard. The Surface probe used had the probe axis normal to the surface. The probe was connected to the

instrument using the cable. The device was first calibrated using the calibration standards integrated into the instrument using 14.73 MS/m and 35.78MS/m external standards. The probe was placed on the specimen and held on it steadily until the conductivity value appeared in the display of the instrument. All measurements were carried out in touch mode, under Programme-5 with a frequency of 60HZ and at room temperature. Eddy current response is greatly affected by the test frequency chosen, fortunately this was one property that was controlled. For each specimen, 6 readings were taken and the average conductivity computed.

3.6 The Tensile Test

From the extruded bars of alloys A3 and A12, which had already been subjected to appropriate heat treatment as outlined in page 45 section 3.2 four tensile test specimens of each alloy were machined having a gauge length of 30mm, thickness 1.8 mm and width 13.2mm. All the specimens had been aged to peak hardness before being cut/shaped as shown in Figure 3-6. Machinery of the standard tensile test piece (see Figure 3-6) was done after appropriate heat treatment, and not before, to prevent any deformation zone that may go through recrystallisation and abnormal grain growth. For comparison purposes, a specimen AA6082 (T4 as extruded) was also subjected to the tensile test. Unlike A3 and A12, AA6082 contained dispersoids.

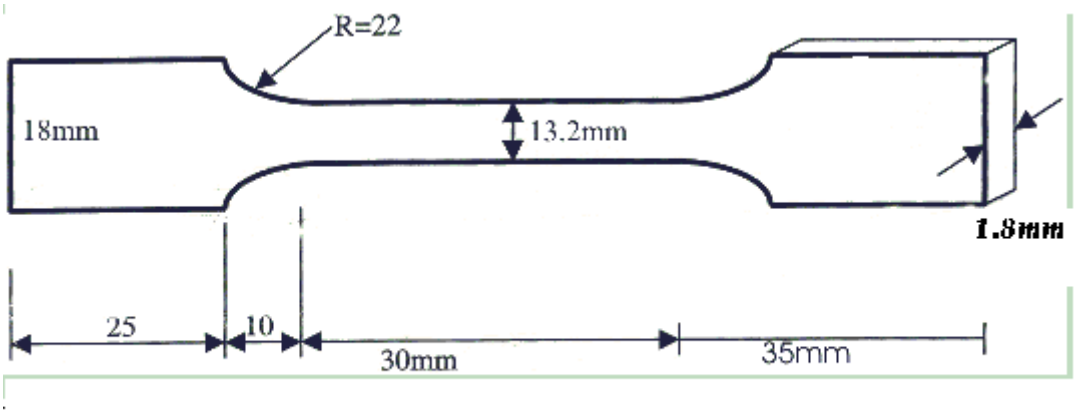

Figure 3-6 Tensile test specimen

Mechanical tensile testing for each sample was carried out at room temperature on a universal testing instrument (model No. 1125, instron tensile testing machine) at a ramp rate/speed of 2mm/min. The ends of each test piece were fixed into grips, one of which is attached to the load-measuring device on the tensile machine, and the other to the straining device. The specimen was subjected to a continually increasing uniaxial tensile force (load) until it fractured. The gauge length was 30mm, which was large enough to accommodate a tensile extensiometer. The extensometer gripped the specimen using a system of sprung knife-edges. The separation of the knife-edges was 25mm. The load and elongation were measured simultaneously at frequent intervals and a plot of load versus extension was recorded autographically during the test and were expressed as average stress and strain according to the equations (2-1) and (2-2). The data obtained from the tensile test is shown in Table 7-1 and was plotted as a stress / strain curve shown in

Figure 4-14. Ultimate tensile stress (also called tensile strength), Yield stress at 0.2% offset, modulus of elasticity and elongation at fracture were determined. The Permanent extension of the gauge length after fracture, was expressed as a percentage of the original gauge length L_0 where L_0 has been taken equal to 30 mm. Elongation is the simplest and most common representation of the ductility of the material.

3.7 TEM specimen preparation

Based on the results obtained from hardness measurements (Section4.2 and Figure 4-12), the samples corresponding to peak hardness in each of the four cases were prepared for TEM studies. They were first ground to foil thickness (~100μm) and then cut to disks of diameter ~3mm using a gatan mechanical punch. 10 to 15 disks of each foil were prepared They were further prepared by conventional electro-polishing using a Struers Tenupol 3 unit with an Electrolyte consisting of 1/3 HNO_3 in 2/3 Methanol. The electro-polishing was done at a temperature range between -25°C and -35°C, using a current of 2.5 A, Voltage 20 V, flow rate 7 and time set to infinity (∞). This temperature range was maintained by adding Liquid nitrogen into the electrolyte. Materials for TEM had to be specially prepared to thicknesses

which allow electrons to transmit through the sample, much like light is transmitted through materials in conventional optical microscopy.

3.8 Microscopy and EELS

All TEM investigations were carried out using a Philips CM 30 TEM equipped with a Gatan parallel EELS system. When measuring the density of the precipitates a critical issue in the analysis is that the thickness of the foil is determined as accurately as possible. In the present investigation, the specimen thickness was measured using Electron Energy Loss Spectroscopy (EELS), which is an effective and reliable method. EELS made it possible to measure the thickness of each sub grain where the density of precipitates was measured. The density of precipitates (the number of particles per unit volume, ϱ) was measured by counting the number of particles (N) in a volume, V=A × t, where t is the thickness of the foil and is obtained by multiplying the the value obtained from EELS with 111nm since $\lambda_{150Kv}^{Al} = 111nm$ (see page 42 section 2.12.3 for details) and A is the projected area of V. The TEM was operated at 150kV to avoid beam damage to the specimen. Each specimen was first tilted to the Al [100] zone axis before any measurements were done. The reason being that the precipitation of Mg-Si metastable phases are present in the form of needles oriented parallel to the three <100> directions in the Al matrix. Pictures of the specimen showing particles, needles and cross sections were taken.

3.9 Measurement of Microstructure

Transmission Electron Microscopy was used for precipitate identification, population and size evaluation.

3.9.1 Length of the needles (L)

The length, L, of needles was measured on the TEM pictures using a ruler. The actual length, ℓ, was determined from the formula

$$l = \frac{L}{M} \qquad (3\text{-}2)$$

Where M=magnification x10^3

For each specimen, 300 to 500 needles were measured from TEM negatives and the average length computed. Except for specimen A12/570/17h where the magnification used was 89K and A12/520/17h where the magnification used was 120K, all the other specimen pictures for needle length measurement were taken at a magnification of 260K

3.9.2 Number density (N)

The number density of the precipitates was visually counted on TEM negatives. Only particles /needles in the zone axis direction i.e. the spots in the <100> direction perpendicular to the paper plane was counted. For each sample 10 to 15 bright field images from different grains were recorded and analysed. The analysed images were only from the interior of the selected grains. For number density measurements, a magnification of 260K was used for all specimens except A12/570/17h where a magnification of 160K was used.

3.9.3 Cross Section area (CS)

From each specimen, 25 to 100 cross sections of particles were measured and the average computed. Due to the irregular shapes of the particles, it was very difficult to compute the cross sectional areas of the precipitates. Depending on the shape of the particles, the cross sectional areas was calculated from one of the following formulaeFor circular cross sections

$$CS = \frac{\pi d^2}{4M^2} \qquad (3\text{-}3)$$

The diameter, d, of all circular cross-sections of precipitates was measured using a millimeter scale embed in a magnifying glass.Rectangular or parallelogram cross-section:

$$CS = \frac{a \times b}{M^2} \qquad (3\text{-}4)$$

For the rectangular or parallelogram cross-sections, the longest side, a, and the shortest side, b, of the precipitates were measured using a millimetre scale mounted on a magnifying glass. All pictures taken for purposes of cross section measurements were taken at a magnification of 600K.

3.9.4 Particle Density (ϱ)

The particle density is a measure of the number of particles per unit volume of the sample. The formula used to calculate the particle density is given below:

$$\rho = \frac{3N}{A\left(t + \langle l \rangle\right)} \tag{3-5}$$

Particle density without length corrections were calculated using the formula:

$$\rho_{uncorr} = \frac{3N}{At} \tag{3-6}$$

The number density, N, was multiplied by 3 to account for all the three orthogonal particle directions in the sample. The volume was given by the product of count area, A, and the thickness, t , of this area. The sample thickness was obtained by the EELS method, but the effective thickness was larger by the mean needle length $\langle l \rangle$, because needles having centres up to $\langle l \rangle / 2$ on each side of the specimen were counted. The particle density using length corrections is therefore given by equation (3-5)

3.9.5 Volume Fraction (VF)

The Volume Fraction gave the amount of alloying elements that formed precipitates in the sample.

$$VF = \langle CS \rangle \langle l \rangle \langle \rho \rangle \tag{3-7}$$

4 CHAPTER 4 RESULTS AND DISCUSSION

4.1 Grain Size

The initial grain size of the material is important for the subsequent heat treatment, and for the resulting mechanical properties, especially yield stress and ductility. These macroscopic properties are a direct result of the microstructure (e.g. grain size and hardening precipitation phases). The initial grain size of the as extruded alloys was measured using the linear intercept method in the optical microscope. The grain size distribution at the surface and and at a distance of 8 mm from the surface were found to be different. The mean intercept sizes of the as-extruded specimens were found to be 57.9μm and 78μm for alloys A3 and A12 respectively when measured at 8 mm below the surface. At the surface, the mean grain intercept was found to 37μm and 55μm for A3 and A12 respectively.

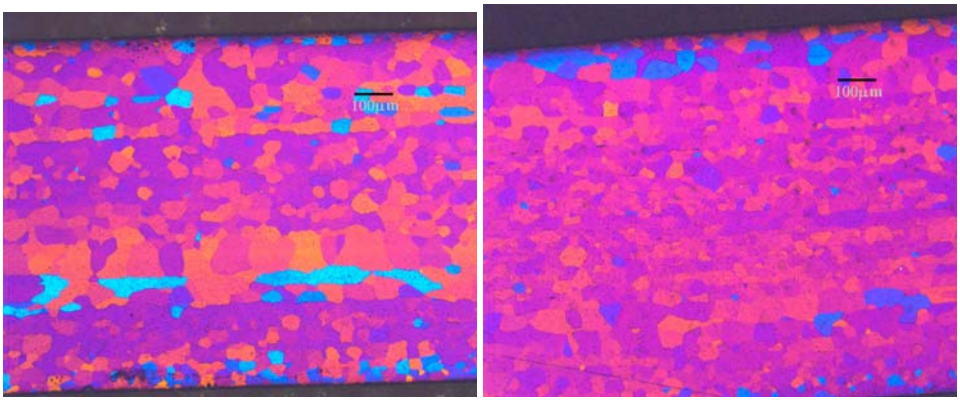

(a) (b)

Figure 4-1 Micrographs of the as-extruded-grains of alloys A12 and A3

The grain structure of the two alloys subjected to the solution heat treatment as outlined in section 3.2 were aged to peak hardness (see Figure 4-12) and were monitored before and after deformation by tensile test. All the investigations were carried out at the narrowest surface as shown in Figure 4-2 at a distance of 8 mm from the surface and in the centre of the specimen in the extruded direction. The deformed specimens were examined at a distance of 3 mm from the deformation surface and in the same orientation as shown below. The micrographs to the

right were taken after deformation by tensile test. The ones on the left were taken before deformation.

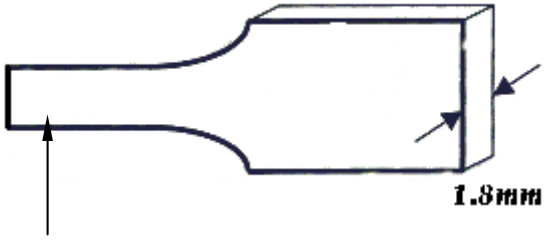

Figure 4-2 Figure showing the orientation of grain size measurement. The arrow shows the position where the grain size was measured

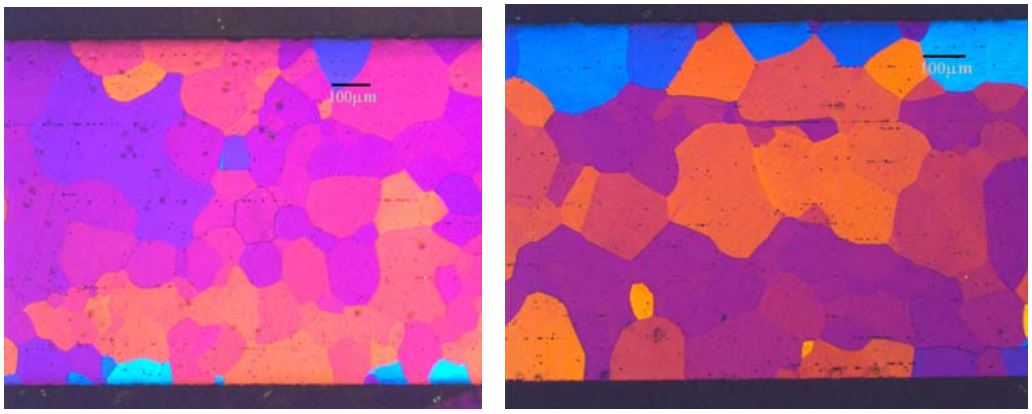

Figure 4-3 Micrographs of the grains of A12/520/17h before and after deformation by tensile test.

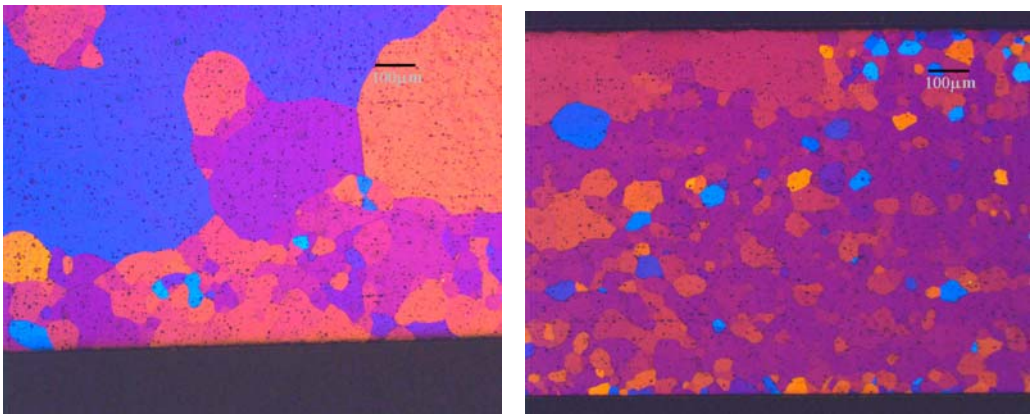

Figure 4-4 Micrographs of the grains of A3/520/17h before and after deformation by tensile test.

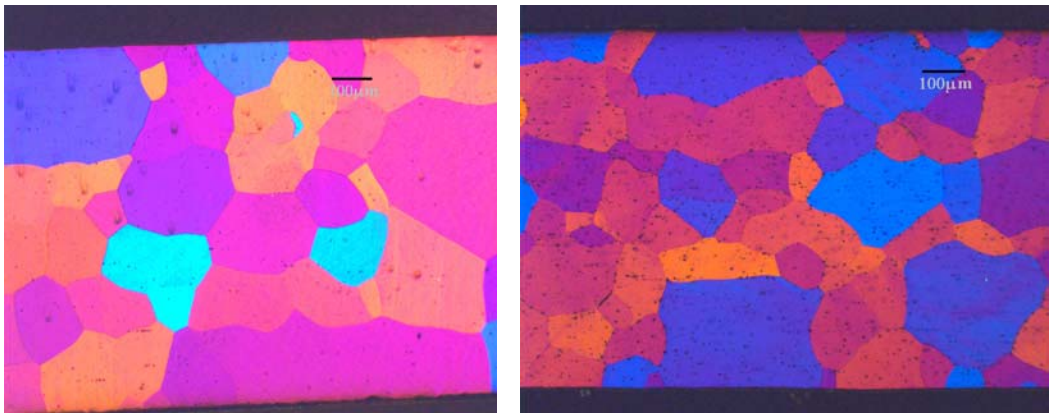

Figure 4-5 Micrographs of the grains of A3/570/17h before and after deformation

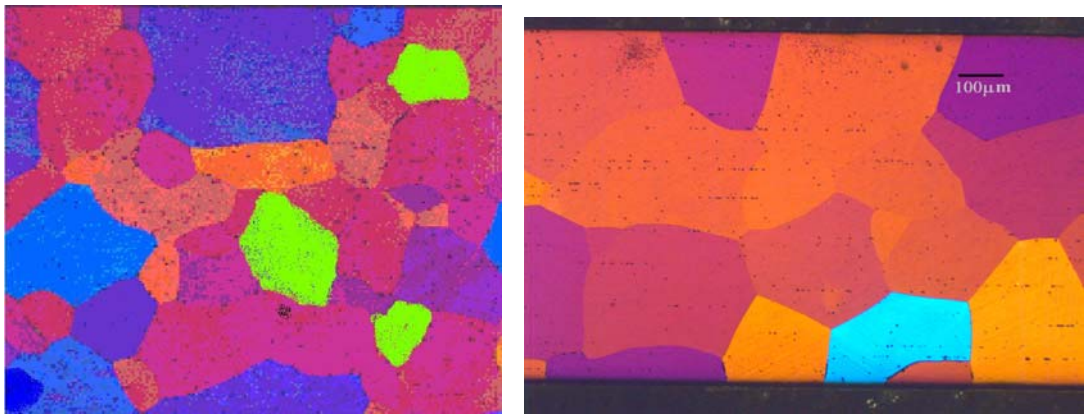

Figure 4-6 Micrographs of the grains of A12/570/17h before and after deformation by tensile test

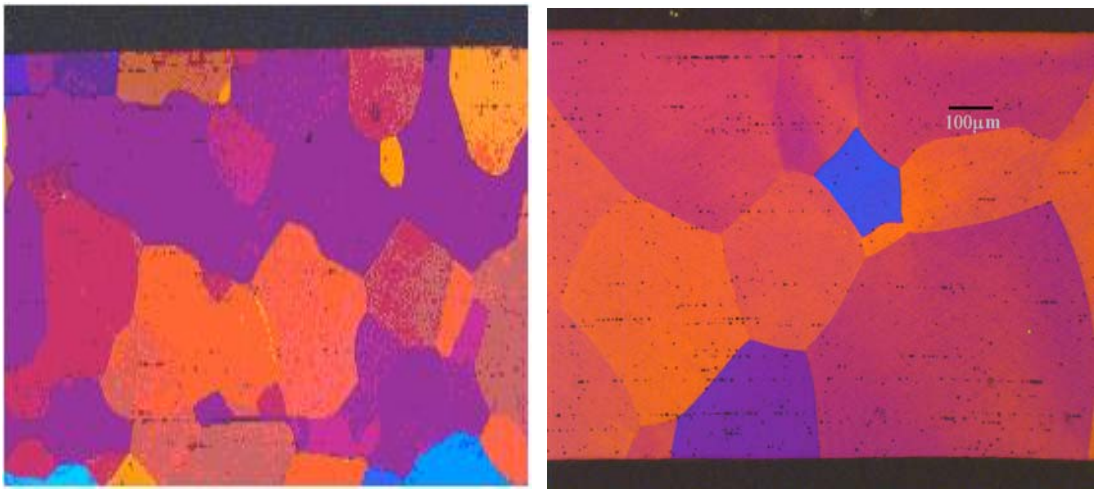

Figure 4-7 Micrographs of the grains of A12/570/3h before and after deformation by tensile test

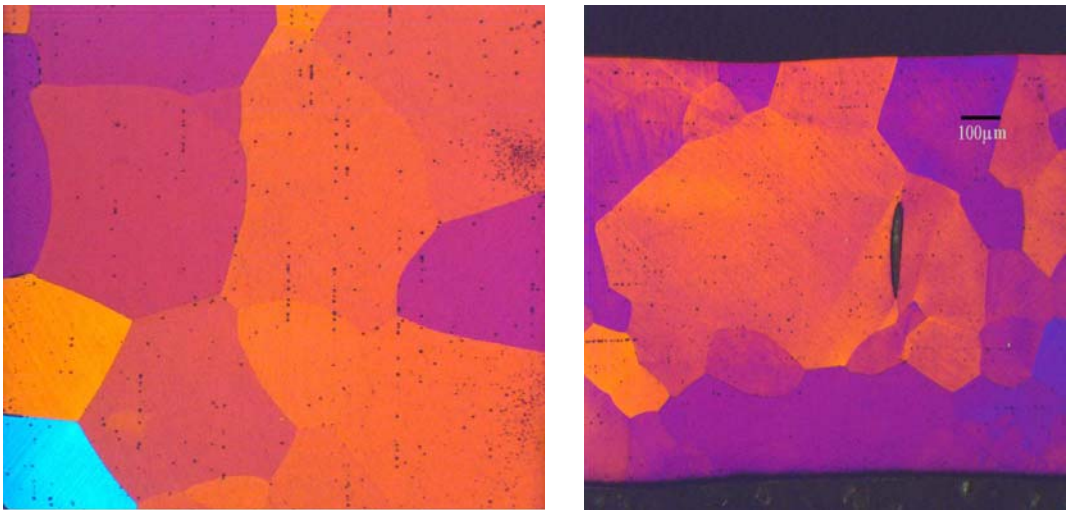

Figure 4-8 Micrographs of the grains of A12/520/3h before and after deformation by tensile test

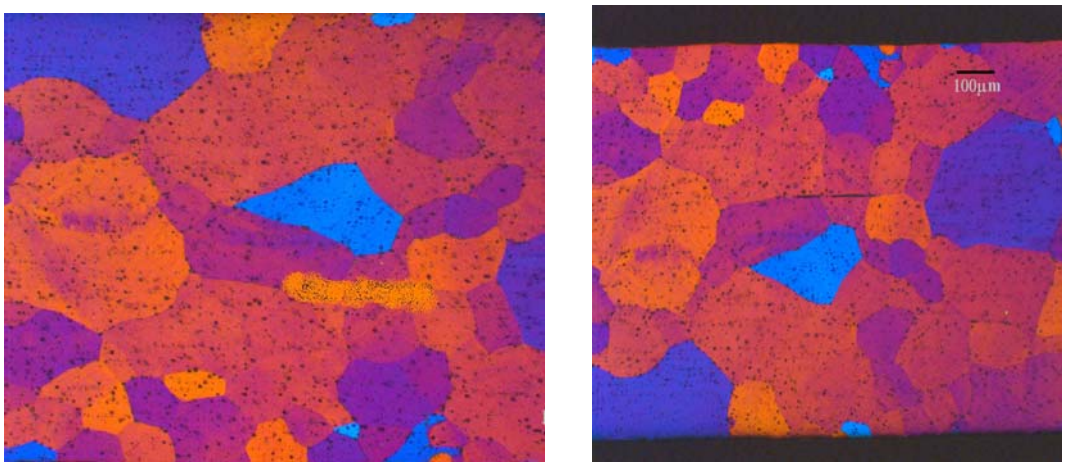

Figure 4-9 Micrographs of the grains of A3/570/3h before and after deformation by tensile test

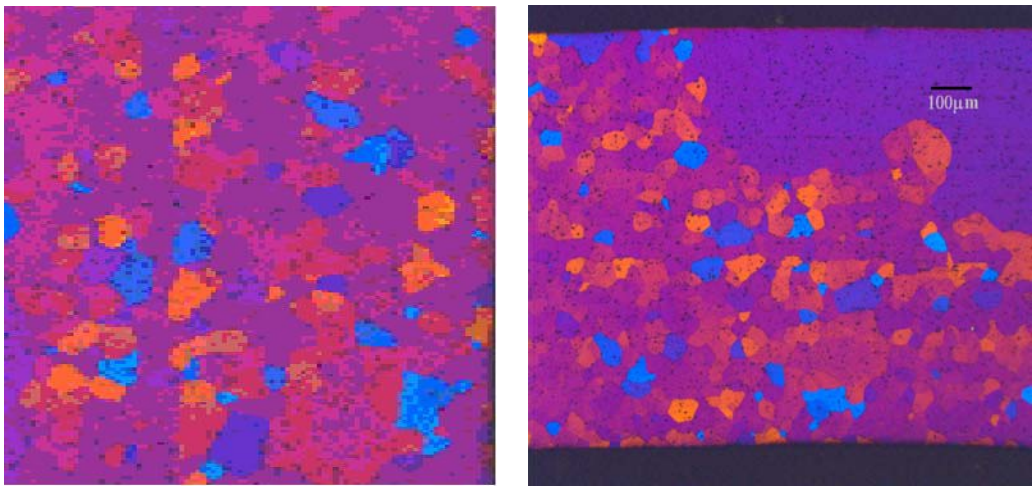

Figure 4-10 Micrographs of the grains of A3/520/3h before and after deformation by tensile test

The grain diameters of the investigated specimens are summarised in Table 4-1. The results of grain sizes did not agree with Hall-Petch equation. According to the Hall-Petch relationship (see equation (4-1) on page 34) reducing the grain size increases the alloy strength (yield strength).i.e. a linear relationship between flow stress and the reciprocal of the square root grain diameters. Equation (2-7) shows that strength is directly proportional to the reciprocal of the square root of the grain diameter. On the controrary our results indicate that as the grain size increases the yield stress increases too. We can easily say that the grain size does not affect the tensile properties at all. However it is true that A3 has a slightly more fine grain structure than A12. The fact that Grain size does affect the strengthening of A3 and A12 according to the findings was also confirmed by Prof. Engler Olaf in his talk entitled Strengthening mechanisms in Aluminium. I quote him, "Grain size is not an important parameter in Aluminium alloys as far as strengthening is concerned."

4.2 Tables of Experimental results

Table 4-1 Data for Grain Size measurement taken at 8 mm below surface

Sample description	Mean grain size before deformation by Tensile test (μm)	Mean grain size after being deformed Tensile test (μm)
A3 as Extruded	58	-
A12 as Extruded	78	-
A12/520/3h	132	378
A12/520/17h	222	362
A12/570/3h	330	775
A12/570/17h	336	346
A3/520/3h	109	129
A3/520/17h	331	347
A3/570/3h	119	309
A3/570/17h	358	362

Discussion on Grain size

Table 4-2 Relating Grain size and yield strength/Hardness

Specimen	Grain Size (μm)	Yield Stress (Mpa)	Hardness (HV1)
A3/520/3h	109	219	109.8
A3/520/17h	331	259	107.9
A3/570/3h	119	212	102.7
A3/570/17h	358	263	103.1
A12/520/3h	132	192	92.5
A12/520/17h	222	265	109
A12/570/3h	330	162	88.8
A12/570/17h	336	230	108.9

Below I show the relationship between the yield strength and grain size (see table Table 4-2). In particular take note of the fact that the grain size of A3/570 after 3 hours annealing time is slightly smaller than the grain size of A3/570 after 17 hours annealing time. Paradoxically the yield strength of A3/570 after 3 hours annealing time is also smaller than the yield strength of A3/570 after 17 hours annealing time. This result is in total disagreement with the Hall-Petch equation.

For any given alloy treated at a particular solution temperature, when the grain size increased, there was a corresponding increase in yield strength. This is not consistent with the Hall-Petch equation which demands that reducing the grain size increases the alloy's yield strength according to equation (2-7).

For any given annealing time, the Si-rich alloy (A3), when solution heat treated for 10 minutes at 520ºC produced a slightly smaller grain size than when it was solution heat-treated for 2 hours at 570ºC. This is also true for the Mg-rich (A12) alloy. Except for the grain sizes of A3/520/17h and A3/570/17h the trend here seemed to favour the Hall-Petch demand that the smaller the grain size the higher the alloy's strength.

In general, A3 had a more fine grain structure than A12 before being subjected to any heat treatment. After heat treatment however, this was not necessarily true e.g. the grain size of A3/520/17h was 331μm while that of A12/520/17h was 222μm. Also the grain size of A3/570/17h was 358μm while that of A12/570/17h was 336μm.

RECRYSTALLIZED GRAIN SIZE

Upon heat treatment, the alloys were recrystallised. Some earlier research points out that w hen the grain size becomes macroscopic in dimension, the number of grains in a test piece may be so few that the material acts more like a single crystal than a polycrystal. In those instances, the strength in a particular stress direction may be substantially higher or lower than in a material having a normal grain size[13.p 125]

Table 4-3 Results of the mean values of Vickers Hardness after ageing at 175 °C

Time (hrs)	SPECIMEN			
	A12/570	A3/570	A12/520	A3/520
	MEAN HV	MEAN HV	MEAN HV	MEAN HV
0.5	64.6 ± 0.37	65.7±0.79	69.08±0.91	67.07±0.72
1	68.1 ± 0.46	72.8±1.04	72.68±0.63	79.45±1.12
2	77.0 ± 0.51	91.2±0.59	80.95±0.75	95.33±1.44
3	88.8 ± 0.87	102.7±0.77	92.46±1.19	109.84±1.35
4.5	94.1 ± 0.53	99.8±0.54	97.42±1.01	110.03±0.67
6	101.4±0.83	105.3±1.49	100.2±0.80	106.1±0.96
10	106.5±1.07	104.3±3.87	103.45±0.65	112.18±1.32
17	108.9±1.38	103.1±0.81	109.03±0.28	107.97±1.34
24	101.9±1.19	99±1.93	103.22±0.67	106.24±0.90
36	91.87±0.95	93.1±1.48	97.5±0.98	96.5±1.67
100	79.9 ± 0.8	87.1±1.74	75.6±0.77	86.5±0.62
200	70.4 ± 0.95	73.9±0.83	68.5±1.04	78.1±0.91

Table 4-4 Results of the mean values of electrical conductivity

Time(hr)	SPECIMEN			
	A12/520	A3/520	A12/570	A3/570
	MEAN σ(MS/m))	MEAN σ(MS/m))	MEAN σ(MS/m))	MEAN σ(MS/m))
0.5	27.4±0.14	27.5±0.00	27.63±0.09	27.87±0.06
1	27.5±0.10	27.7±0.03	27.63±0.09	28.50±0.00
2	27.6±0.05	28.3±0.16	27.57±0.03	28.60±0.03
3	28.1±0.06	29.5±0.15	28.00±0.00	29.17±0.09
4.5	28.4±0.00	29.0±0.08	28.76±0.11	29.90±0.06
6	28.6±0.12	29.4±0.03	29.04±0.20	29.78±0.13
10	30.4±0.07	30.0±0.10	30.07±0.07	30.53±0.07
17	30.5±0.07	30.2±0.00	32.00±0.11	30.40±0.12
24	31.4±0.07	30.4±0.03	32.28±0.11	30.80±0.00
36	32.2±0.12	32.0±0.06	32.65±0.09	31.00±0.00
100	33.4±0.00	31.1±0.06	33.43±0.08	31.80±0.00
200	33.6±0.06	31.7±0.10	33.5±0.06	32.33±0.07

4.3 Graphs

This section presents the experimental graphs

4.3.1 Ageing at Room temperature Curve

The figure below shows hardness curves for A3 and A12 after solution heat treatment at 570^{0}C for 2 hours (or 520^{0}C for 10 minutes) and during the 4 hours of storage at room temperature. Samples labelled AX/520 were solution treated at 520^{0}C for 10 minutes while those labelled A12/570^{0}C were solution treated at 570^{0}C for 2 hours before they were quickly quenched in water and stored at room temperature for 4 hours The broken curves represent alloy A12 while the solid lines represent A3. The composition of the investigated alloys is shown on page 44 in Table 3-1.

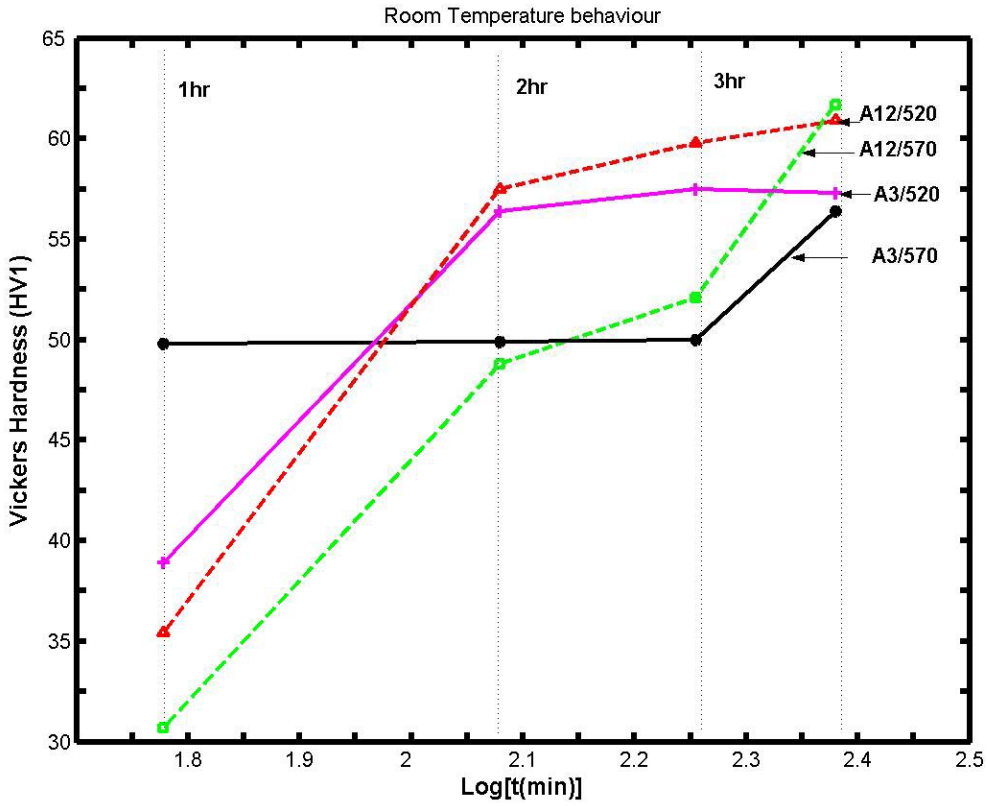

Figure 4-11 Ageing behaviour at room temperature

4.3.2 Hardness Curves

The evolution of hardness as a function of annealing time is shown in Figure 4-12.The hardness curves of the investigated alloys is compared under two different solution heat treatments (but same annealing temperature and time). The solid curves represent the alloys that were solution heat treated at 570^0C for 2 hours while the broken curves indicate the hardness of the alloys that were solution heat treated at 520^0C for 10 minutes.

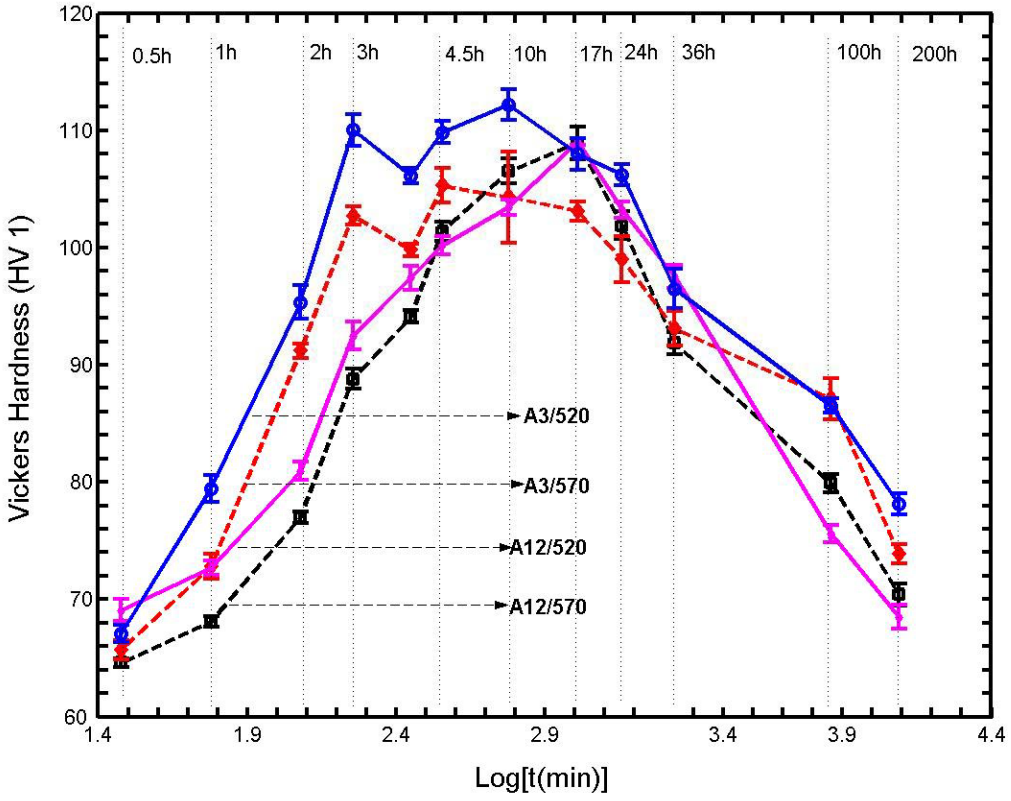

Figure 4-12 Vickers Hardness as a function of isothermal annealing time at 175°C for different solution heat treatments. Samples labeled AX/520°C were solution heat treated at 520°C for 10minutes while the AX/570°C were solution heat treated at 570°C for 2 hours. All samples were held at room temperature for 4 hours prior to being annealed

4.3.3 Electrical Conductivity curves

Electrical Conductivity of all samples was measured by an eddy current technique, and inferences were then drawn about the different factors affecting conductivity, such as material composition, heat treatment and solute elements. The conductivity curves for the alloys A3 and A12 is compared under two different solution heat treatments (but same annealing temperature and time) and are presented Figure 4-13

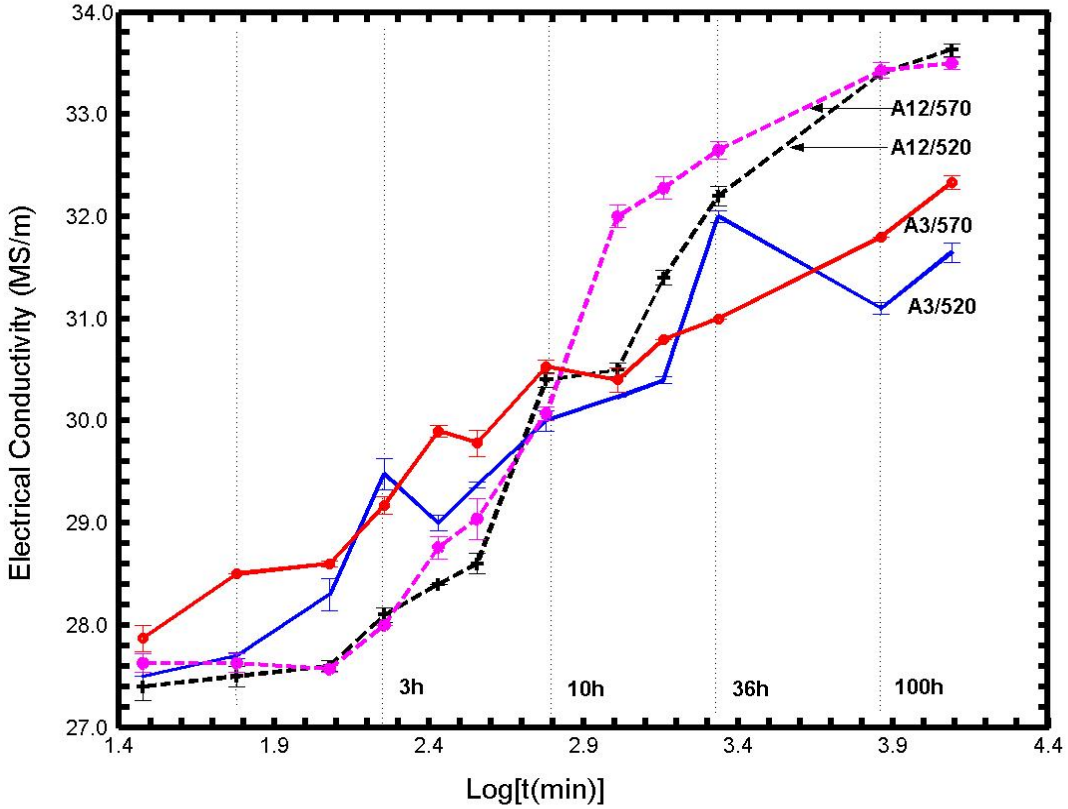

Figure 4-13 Electrical Conductivity for samples A3 and A12 as a function of isothermal annealing time at 175°C for different solution heat treatments. AX/520 means the sample was heat treated at solution temperature of 520°C for 10minutes while AX/570 a solution temperature of 570°C for 2 hours. All samples were held at room temperature for 4 hours prior to annealing

4.3.4 Stress-strain Curves for investigated alloys

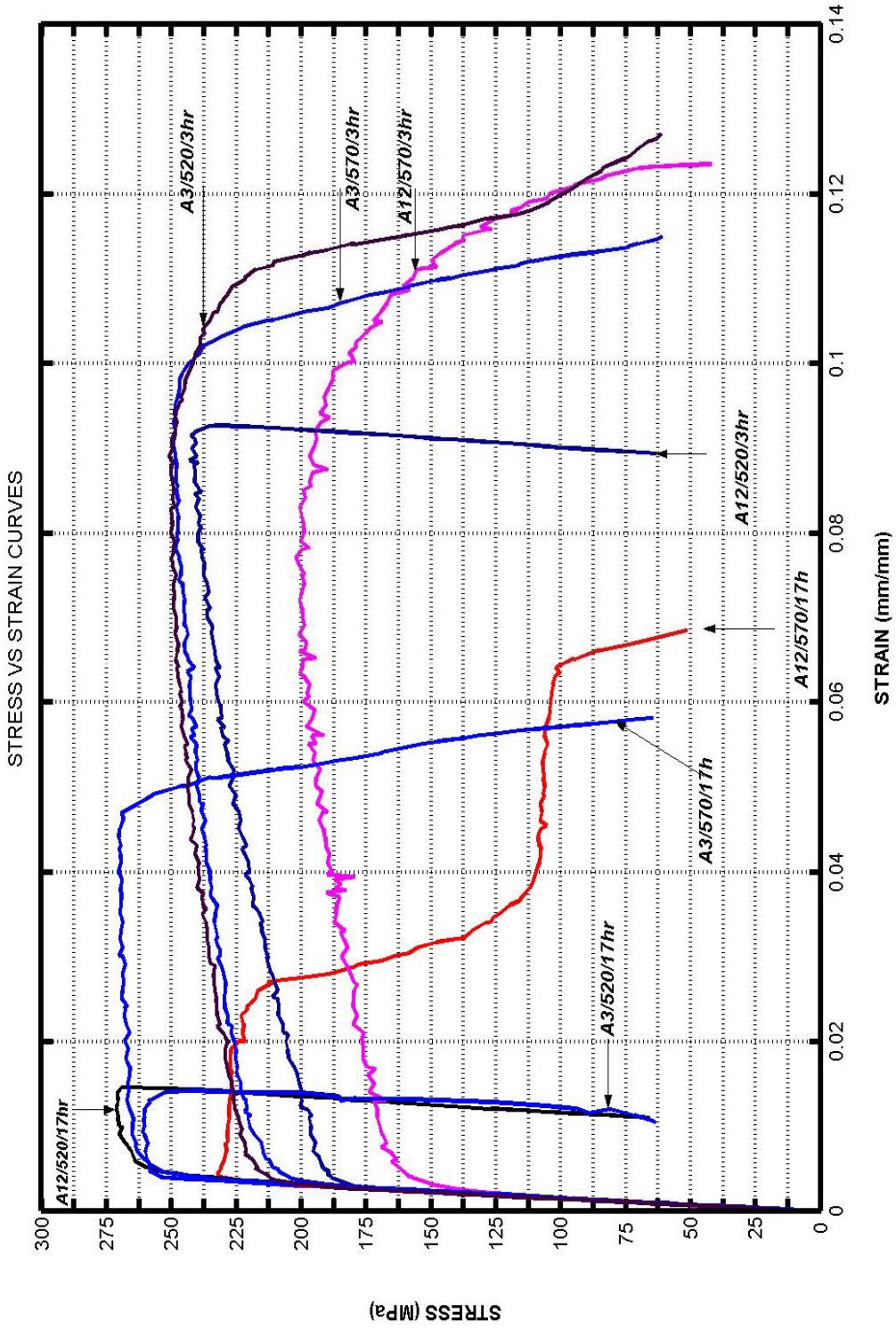

Figure 4-13 Stress – Strain curves for specimens corresponding to peak hardness

Figure 4-14 Stress – Strain curves for specimens corresponding to peak hardness

4.3.5 Stress-strain curve for AA6082

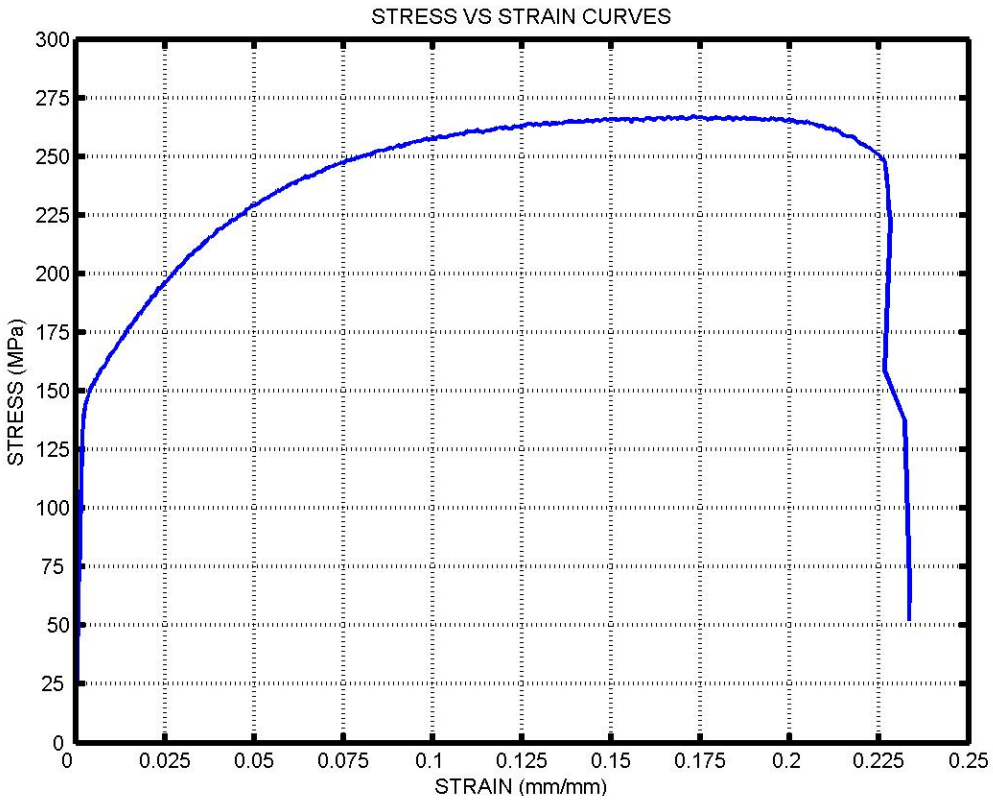

Figure 4-15 Stress-Strain Curve for AA6082 (T4 as extruded) Alloy

Figure 4-15 shows the stress-strain curve for AA6082 (T4 as extruded and contains dispersoids). This experiment was done for purposes of comparison with the investigated dispersoid free alloys A3 and A12.

4.4 Microstructural Examination by TEM

According to the results of hardness measurements (see Figure 4-12) and tensile tests (seeFigure 4-14), two solution heat treatments as out lined in section 3.2 and one aging conditions have been selected to carry out micro structural examination. The microstructures of the 2 alloys aged at 175°C for 3 hours and others for 17 hours have been examined by TEM. Although of different compositions (see Table 3-1), both alloys had a high purity i.e. they did not contain any dispersoids. Both alloys in all conditions contained needle-like shaped precipitates examples being GP zones, β" etc (see Figure 4-16 through Figure 4-19).

Comparison between A12/520°C /3h and A3/520 °C /3h

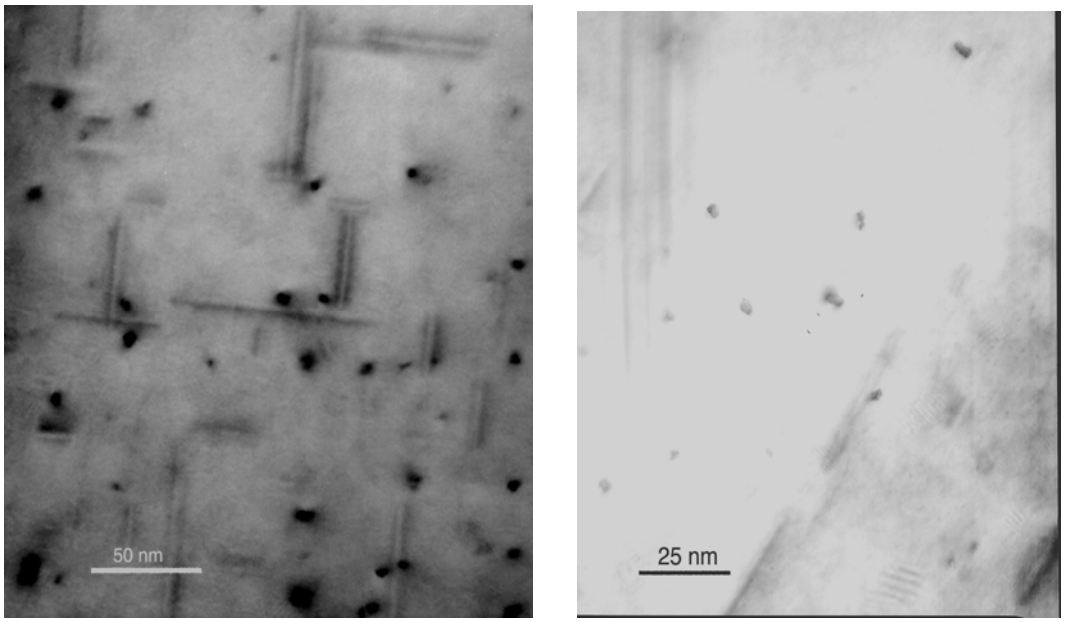

A12/520 /3h

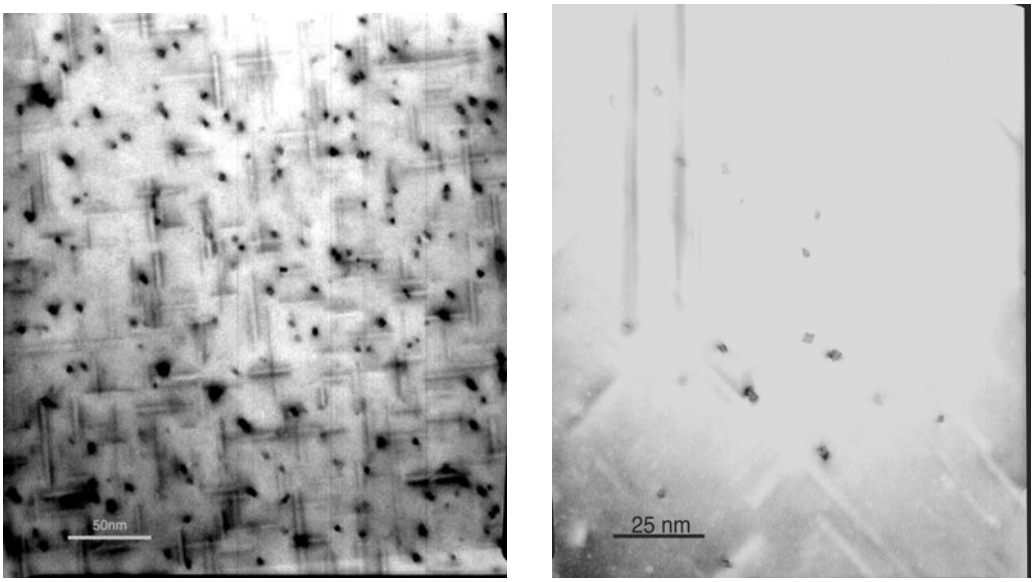

A3/520 /3h

Figure 4-16 TEM bright field images of A3/520/3h and A12/520/3h. A lower number density of precipitates in Mg-rich (A12) corresponds to a coarse microstructure.

Comparison between A12/570 °C /3h and A3/570 °C /3h

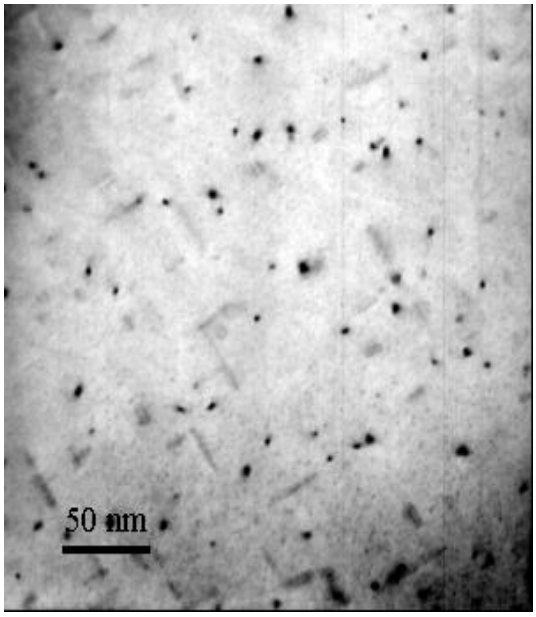

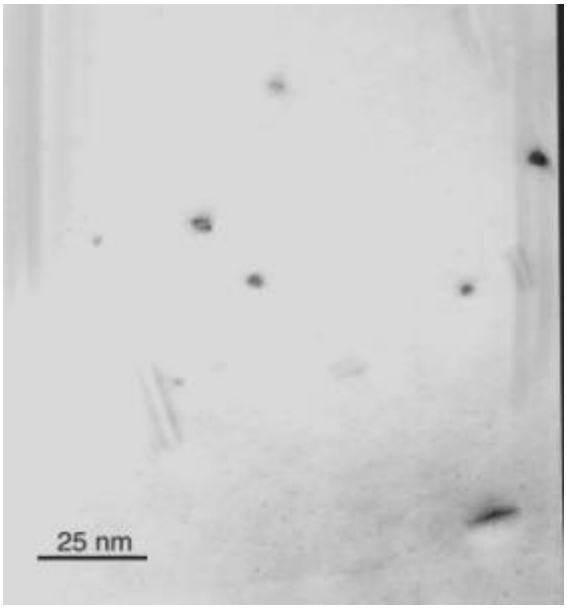

A12/570 /3h

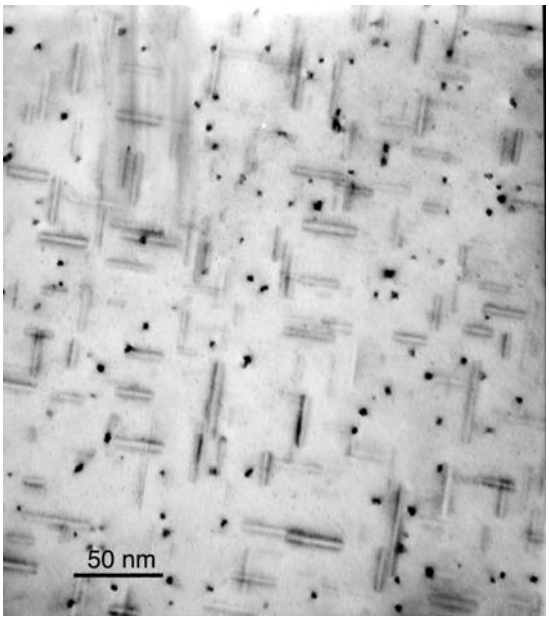

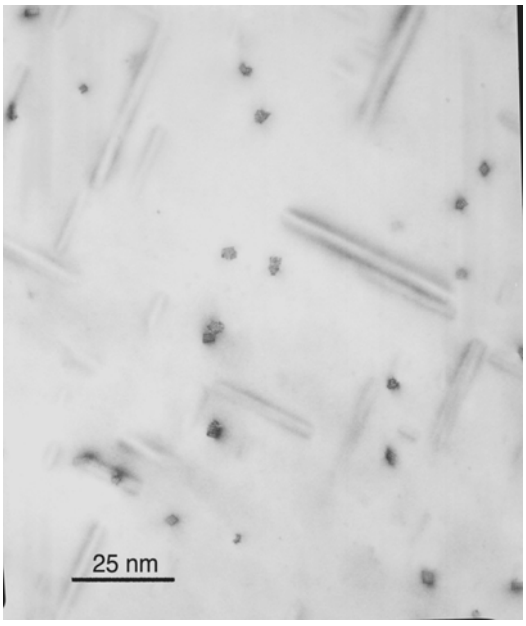

A3/570/3h

Figure 4-17 TEM bright field images of A12/570/3h and A3/570 /3h. A lower number density of precipitates in Mg-rich (A12) corresponds to a coarse microstructure

Comparison between A12/520 °C /17h and A3/520 °C /17h

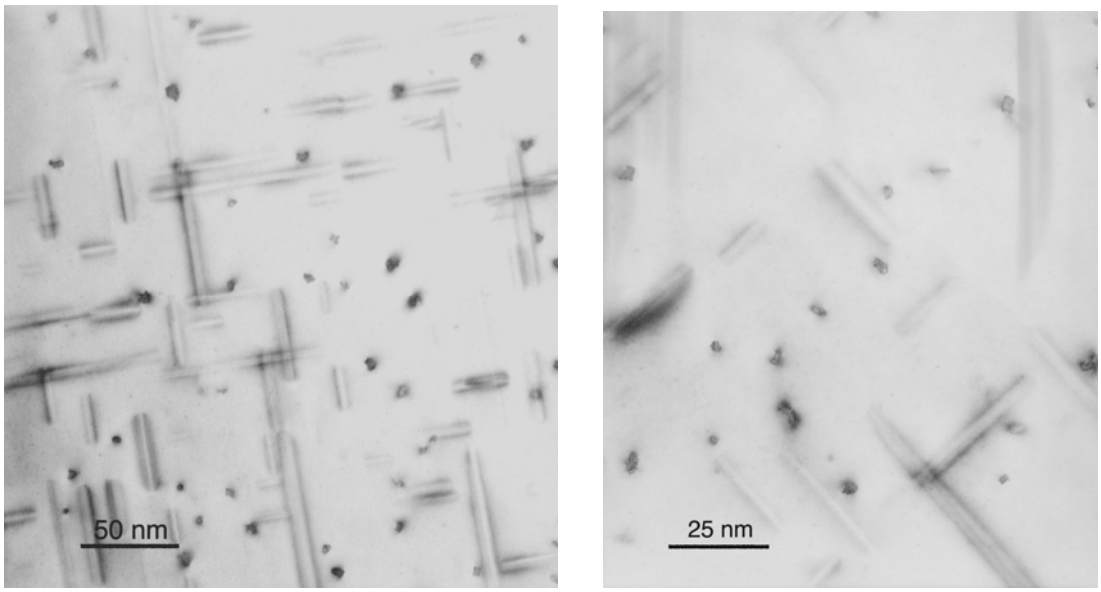

A12/520/17h

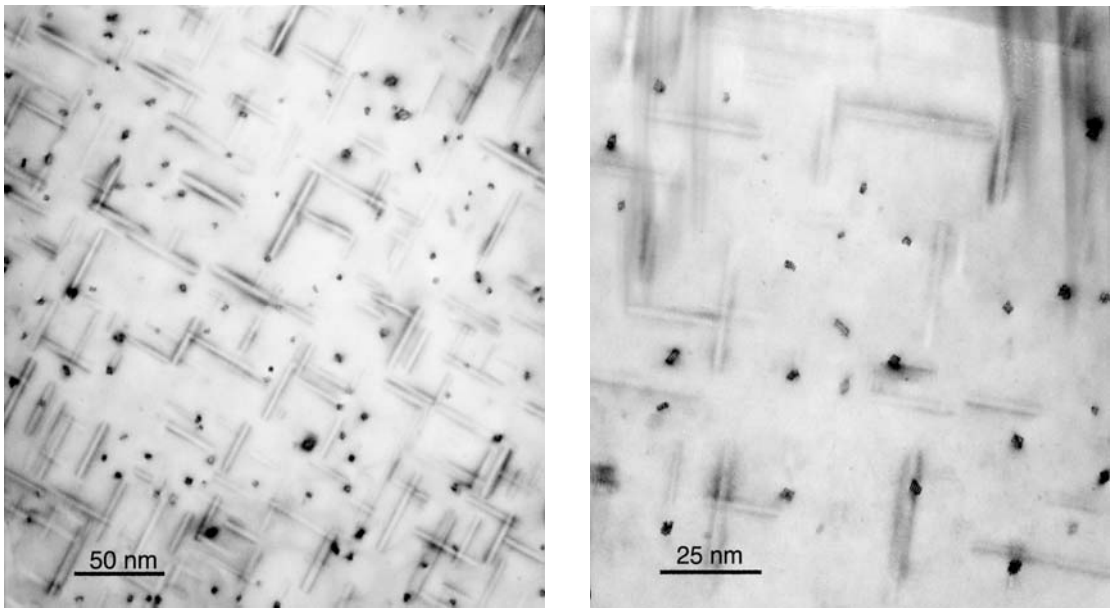

A3/520 /17h

Figure 4-18 TEM bright field images of A12/520 °C /17h and A3/520 °C /17h. Note the Longer needle lengths in Mg-rich (A12) alloy.

Comparison between A12/570 °C /17h and A3/570 °C /17h

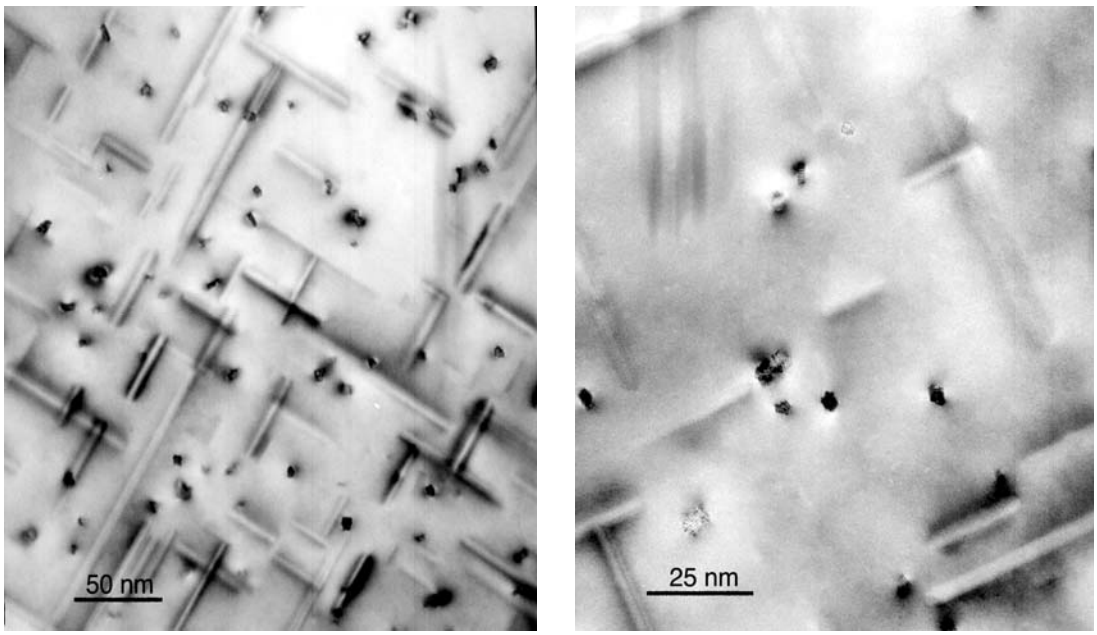

A12/570 /17h

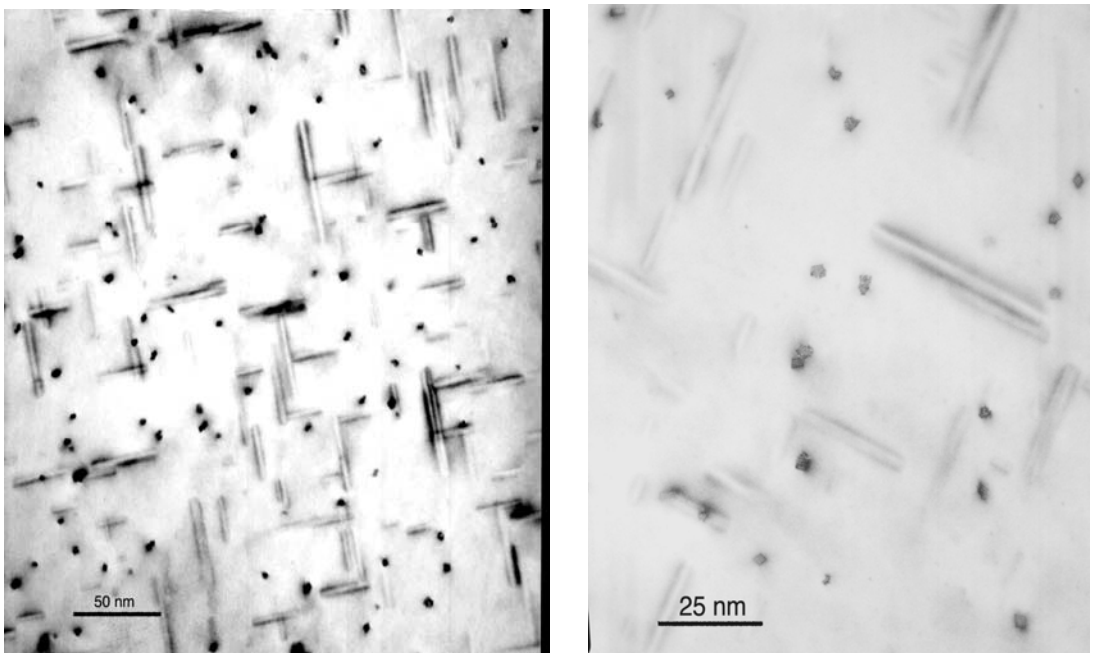

A3/570 /17h

Figure 4-19 TEM bright field images of A12/570/17h and A3/570/17h. Note the Longer needle lengths in Mg-rich (A12) alloy.

Phases observed in A3/520/3h and A12/520/17h

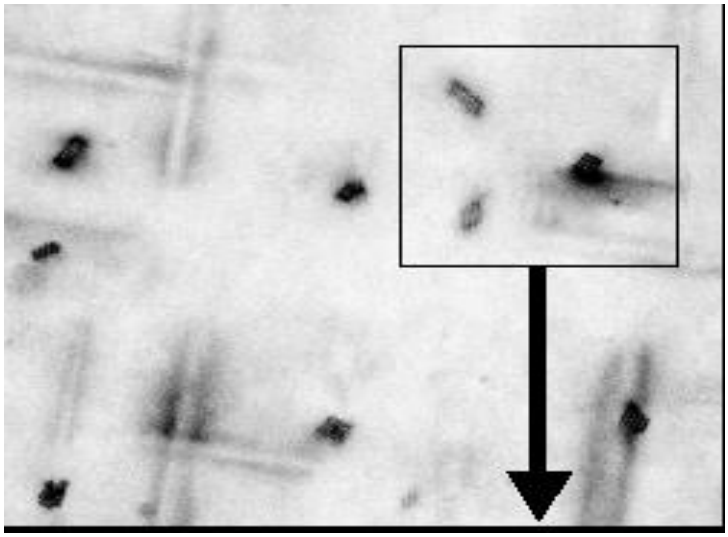

Figure 4-20 β" precipitates in A3/520/17h

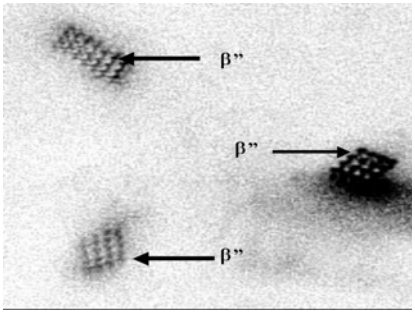

Figure 4-21 β" phase magnified from box in Figure 4-20

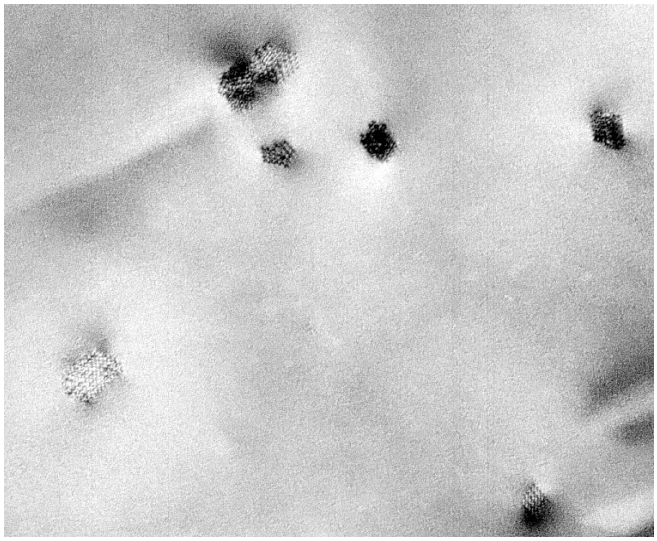

Figure 4-22 Different phases in A12/570/17hr (see the U-phase to your lower left)

Table 4-5 Average cross sections, lengths, particle densities and Volume Fraction after different aging times at 175°C for A3 and A12

Specimen	$\langle l \rangle$ (nm)	$\langle cs \rangle$ (nm^2)	$\langle \rho \rangle_{corr}$ (part/μm^3)	VF
A3/520/3h	27.6±0.61	3.45±0.12	34508±836	0.33%
A3/570/3h	28.0±0.5	5.2±0.16	32983±895	0.48%
A3/520/17h	31.7±0.84	4.37±0.11	33380±2042	0.46%
A3/570/17h	30.5±0.77	3.52±0.20	32187±1085	0.35%
A12/520/3h	29.2±1.42	5.70±0.26	8682±513	0.14%
A12/570/3h	26.3±0.58	4.64±0.23	9131±595	0.11%
A12/520/17h	50.3±1.46	8.77±0.34	12268±350	0.54%
A12/570/17h	71.3±3.30	11.2±0.50	9207±331	0.74%

$\langle l \rangle$ = Average length $\langle cs \rangle$ = Average cross section $\langle \rho \rangle_{corr}$ = number density VF =Volume Fraction

Results

The sum total of Mg and Si present in the investigated alloys, A3 and A12, was kept constant i.e. Mg + Si =1.3 at % (see Table 3-1). During manufacture, both alloys had been intentionally tailored to have a ratio, $Si/Mg \cong 1$. This ratio is inevitable for creating an alloy with composition close to or same as that of β". The chemical formula of β" is Mg_5Si_6. The β" is the main hardening phase[5] in these kind of alloys. The constant sum, $Mg + Si = 1.3$ at % was maintained for both alloys so that we observe how the microstructural precipitate changes with Si/Mg ratio while vacancy concentration was kept constant by subjecting them to same heat

[5] The reason for the hardening effect is the interface coherency in {001} type Al planes that produces a strong strain field around the precipitates, which slows the movement of dislocations [3] i.e. interface strain that arise between matrix and small, coherent metastable precipitates forming from solid solution.

treatment. Two heat treatments were used to compare microstructural precipitation and resulting macroscopical properties These heat treatments are described in section 3.2 and summarised below. Different solution heat treatment temperatures and time were used to vary vacancy concentration while keeping alloy composition constant.

Two heat treatments were used:-

- **I:** 10 minutes at 520°C , 4hours storage at RT and ageing (0.5-200) hours at 175°C..
- **II:** 2 hours at 570°C , 4 hours storage at RT and ageing (0.5-200) hours at 175°C

4.5 Hardness

Room Temperature behaviour

The hardness of a metal, defined as the resistance to penetration, gives a conveniently rapid indication of its deformation behaviour. For Steel, it has been shown that $3 \times HV = YS$,[11] i.e. when 3 multiply the hardness of steel, it gives its corresponding yield strength. The ageing response of both alloys was monitored using Vickers Hardness testing with a 1 kgf load (see section 3.4). The mean results of the Vickers hardness are summarized in Table 4-3. After solution heat treatment as out lined section 3.2, all specimens were quenched and stored at room temperature for 4 hours. While at room temperature, their variation of hardness with time was monitored and the results are shown in Figure 4-11.

During storage at room temperature a significant hardness increment was observed. The room temperature hardening behaviour shows very similar results to the annealing hardening behaviour. When each alloy was solution treated at 520°C it was found to be harder than when it is solution treated at 570°C for both the room temperature behaviour and the annealing behaviour. The RT storage is necessary for practical reasons. It has a significant effect on precipitates[12]. After solution heat treatment, the solid solution is thermodynamically unstable and during the 4 hours storage at RT, atom clusters form which result in a significant increase in hardness [3]. A long storage time generally produces a coarser final microstructure in Si-rich alloys in particular it lowers the strength of a6082 (T6) alloy [12].

Si-rich (A3) Alloy

For both solution heat treatments, the hardness curves obtained for alloy A3 under isothermal ageing at 175°C are presented in Figure 4-12. Alloy 3 displayed two hardening peaks one after 3 hours and the other after about 10 to 17 hours ageing time at 175°C. For heat treatments I and II the curves for alloy A3 show a similar profile. The first and second peaks for A3/520 are 109 and 112 respectively and for A3/570 was 102 and 104 respectively (see section 3.2 for specimen description). Controrary to expected results, A3/520 showed a higher hardness for the entire ageing period i.e.A3 was hardened most when it was subjected to heat treatment I.

TEM analysis of the samples corresponding to peak hardness revealed the following characteristics:

- A3 has more particle density after 3 hours annealing time than after 17 hours annealing time. This was generally true for both heat treatments.
- A3 produces more particles when it is subjected to heat treatment I[6] than when it is subjected to heat treatment II under standard conditions.
- The average needle length of A3 increased slightly when subjected to either heat treatment. However after 3 hours ageing time, the needle length of A3 under heat treatment I was shorter than its corresponding counter part under heat treatment II.
- The particle cross-sections after 3 hour annealing time is smaller for heat treatment I but the scenario is different after 17 hours annealing time where heat treatment II produces smaller particle cross-sections.
- For both heat treatments and ageing time, volume fraction was below 0.5% even for the hardest specimen.

[6] **I:** 10 minutes at 520°C , 4hours storage at RT and ageing (0.5-200) hours at 175°C.

II: 2 hours at 570°C , 4 hours storage at RT and ageing (0.5-200) hours at 175°C

- Volume fraction for A3 increased with increasing ageing time when subjected to heat treatment I but the reverse was true for heat treatment II.

- At 3 hours annealing time, A3/520 recorded more particle density, less cross-sectional area than A3/570. This may explain why A3/520 has a higher hardness than A3/570.

- The needle lengths of A3/520 and A3/570 are more or less the same for both shorter and longer annealing times.

- The volume fraction for both A3/520 and A3/570 at shorter and longer ageing time never exceeded 0.48%.

TEM pictures showing microstructural precipitates for A3/520/3h, A3/570/3h, A3/520/17h and A3/570/17h are shown in Figure 4-16 through to Figure 4-19 together with their corresponding high magnification images. The dark spots are needles along the <100> aluminium viewing direction. These needles were used for estimating the number densities documented in Table 4-5. The double stripes around the edges of precipitates originate from the interface strain in β" and GP-zones [12]. In A3/520/17h β" precipitates were observed to be ordered with cross-sections having the monoclinic angle and it is very clear from Figure 4-20. When determining the crystal structure for β", the monoclinic angle of the Al super-lattice should be β =105.3° [12].

Using HREM/diffraction techniques in determining relative amounts of various types of precipitates in the same alloys subjected to solution heat treatment of 2 hours at 570°C and same ageing conditions as in the present investigation C:D: Marioara Phd, S. J. Andersen Phd, H:W: Zandbergen Phd and R. Holmestad Phd observed that GP zones were only available in A3 after 3 hours of annealing time and their findings on the effect of alloy composition and aging time on density of β" phase summarised in Figure 4-23.

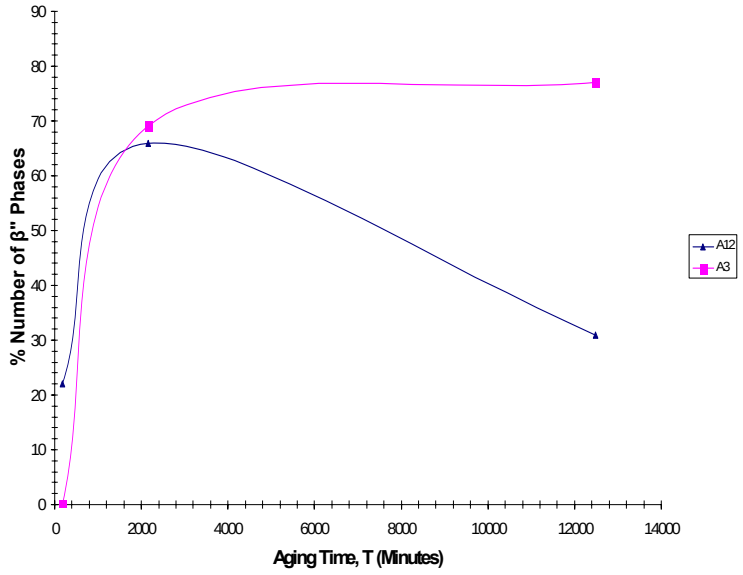

Figure 4-23 Effect of alloy composition and aging time on density of β" [12]

- Therefore, the first hardness peak after 3 hours of ageing time can be attributed to the formation of a high number density of fully coherent GP-Zones. This is evident from Figure 4-23. At 3 hour annealing time, A3 contained only GP-zones and no β" phase.

- The second hardness peak after 10 to 17 hours is caused by slightly fewer but coarser particles, mostly of the β" type. It is clear from the figure that the β" reach a maximum after around 17 hours and this corresponds to peak hardness.

- The higher Si/Mg ratio produced more β" precipitates i.e. A3 produced more β" than A12. In any case A3 was β" optimised.

Mg rich Alloy (A12)

The ageing response of A12 was also monitored for both heat treatments outlined in section 3.2 page 45 The hardness curves showed only one hardening peak after 17hours of ageing time. Both curves show similar profile. The Mg-rich hardness curves are very different from the ones of Si-rich. The peak hardness corresponding to 17 hours annealing time for A12/520 and A12/570 are 109.03 and 108.9 respectively.

TEM analysis of the Mg-rich alloy led to the following conclusions:-

- For both heat treatments, A12 produced very little precipitation of volume fraction less than 0.15% after 3 hours annealing time.

- A12 recorded a much lower particle number density than A3 after 3 hours annealing time for both cases of heat treatments. In general the particle number density is 3 times lower than for the Si-rich alloy for both heat treatments.

- A12 recorded a lower volume fraction than A3 at the beginning of the annealing process and this is very evident from the conductivity graphs (see Figure 4-13)

- However, at longer ageing times, A12 recorded a much more volume fraction than A3. It is clear from Table 4-5 that at 17 hours annealing time A12 recorded a volume fraction of 0.74% compared to only 0.35% recorded by A3 for the same heat treatment. Once again this is confirmed by the conductivity curves.

- At peak hardness ~17 hours annealing time the microstructure of A12 is much more coarser than that of A3 for both heat treatments.

- At 17 hours annealing time, A12 recorded a much longer needle lengths as compared to A3.

- At 17 hours annealing time, A12/520 had a lower volume fraction, higher number density, lower cross-sectional area and shorter needle lengths compared to A12/570.

- At 3 hours annealing time, A12/570 recorded a slightly lower volume fraction higher number density lower cross-section and lower needle lengths.

Discussion

Si-rich alloys generate a high number density of precipitates after short annealing times. This led to a fine microstructure that corresponds to a low volume fraction of precipitates. The volume fraction of Si-rich alloy is lower than that of Mg-rich alloy at longer ageing times. Precipitation is delayed in Mg-rich alloys, the microstructure is coarse and precipitation volume

fraction is lower at shorter annealing times and higher at longer annealing times. The conductivity curves (see Figure 4-13) also confirm the fact that precipitation of Mg-rich alloy is delayed. C. D. Marioara et al gave an explanation to account for this precipitation behaviour and I quote them below. The interactions between atoms and vacancies at the atomic level are responsible for this behavioural pattern. The transformations occurring at the early stages of precipitation involving atomic clustering are crucial for the Mg-rich microstrucure development [12].

It has been observed that quenching a 6xxx alloy immediately after solution heat treatment, separate Si and Mg clusters are present, while Si-Mg co-clusters are developing upon storage at room temperature [12]. Recent research involving atom probe analysis point to the fact the Mg clusters become unstable and dissolve during isothermal heat treatments at temperatures greater than 70°C. On ageing the alloy further, the re-dissolved Mg atoms will enter into Si-Mg co-clusters [12].

The high number of precipitates in Si-rich alloy may be explained from available data on atomic clusters obtained from ion probe analysis experiments. For ageing temperatures exceeding 70°C, a high amount of Si in the alloy will produce a high number of Si clusters and Si-Mg co-clusters. The fraction of clusters with a size exceeding a critical diameter does not dissolve during ageing [12]. Instead, they provide nucleation sites for the subsequent phases, giving rise to a high precipitate number density in the Si-rich alloy. Earlier experimental evidence suggests that the atomic clusters trap vacancies [12] and this may explain why Si-rich alloys exhibit a lower volume fraction of precipitates even at higher ageing times than Mg-rich alloy. It is suggested that the precipitate growth during ageing can be restricted since a fraction of the quenched-in vacancies are trapped by atomic clusters [12].

Although the volume fraction of A3 is low, the hardness of the Si-alloy is higher than that of A12 for both solution heat treatments at 3 hour annealing time and this has been attributed to the high number particle density an the more coherent/semi-coherent interface between the Al-matrix and the small precipitates, as opposed to the larger precipitates[3,8,12,18]. After the 3 hours annealing time, the microstructure of A3 consists of fully coherent GP-zones to transform to β" and other phases having a more semi-coherent interface with the Al matrix.

Despite its low number density, at 17 hours annealing time, the hardness of A12 is slightly more than that of A3 and this is because of the higher volume fraction.in A12.

It is difficult to speculate why A3/520 is harder than A3/570. Similarly, it is not that easy to say why A12/520 is harder than A12/570. At 570°C we expect a higher number of vacancies than can be available at 520°C (more information in section 2.4 vacancies on page 20). So we have more vacancies available for A3/570 than for A3/520. We have a higher number of vacancies available per cluster for Mg and Si diffusion in A3/570 than in A3/520. Considering an imaginary radius for both cases, A3/520 will form more clusters than A3/570. Further more, in A3/520 the radius of the clustering will be less than that of A3/570. Perhaps this may be the reason why A3/520 is harder and records more number density. We can not also rule out the role played by the grain size completely. Maybe it contributes to strengthening effect to some limited degree.

.

4.6 Tensile Stress-Strain Behaviour

Tensile stress-strain properties were measured using specimen design shown in Figure 3-6 page 51. Engineering stress versus engineering strain curves obtained from specimens of A12 and A3 are illustrated in

Figure 4-14 In future discussion, engineering stress will be abbreviated to 'stress' and engineering strain will abbreviated to 'strain'. The non-linearity of the stress strain curves are shown in

Figure 4-14. The initial tangent to the stress-strain curve was used to define Young's Modulus (E), the results are shown in Table 4-6

Table 4-6 Tensile Test Results of specimen A3 and A12

Specimen	E (Mpa)	YS (Mpa)	UTS (Mpa)	EL %
A3/520/3h	65.0	219	251	11.0
A3/570/3h	63.0	212	249	11.0
A3/520/17h	64.6	259	261	1.40
A3/570/17h	64.3	263	270	4.70
A12/520/3h	65.4	192	243	9.10
A12/570/3h	63.9	162	202	12.0
A12/520/17h	62.3	265	271	1.50
A12/570/17h	69.0	230	232	2.80
AA6082 T4	69.0	267	153	22.7

E: Young's modulus, YS: Yield strength, TS: Tensile strength or ultimate tensile strength EL: elongation
Gauge length =30 mm for A3,A12 and AA6082 Cross sectional area = 13.2mm x 1.8mm and 13.2mm x 2.9mm for A3 , A12 and AA6082 respectively.

The tensile strength of an alloy is closely connected to sizes, number density and volume fractions of the GP-zone and β" phases [3,12]. Quantification of these phases for different compositions and thermal histories are therefore important.

The tensile test was conducted to determine:- Tensile Strength, Yield Strength and elongation (Ductility) of each of the alloys under different solution heat treatments but same quenching and aging conditions. The results of yield strength, tensile strength and elongation was then related to alloy composition, annealing time, solution heat temperature, and their microstructure (particle type, size, volume fraction, morphology, number density, etc)

The strain under the A12/520/3hr, A3/570/3hr, A12/570/3hr and A3/520/3hr (here in after referred to as 3hr specimens) curves is greater than that of the A12/520/17hr, A3/520/17hr, A12/570/17hr and A3/570/17hr (here in after referred to as 17hr-specimens). Moreover this indicates that the 3hour- specimens show more elongation than the 17hour-specimens before failure. Ductility is measured by the amount of elongation that can be applied to the material before the failure occurs [2]. 17hour-specimens are less ductile and have more yield strength. On the other hand, 3hour-specimens are more ductile but have less yield strength. The tensile strength for all the 17-hour specimens was observed to be higher than that of 3-hour specimens. We strongly observe here that ductility is sacrificed as strength is increased i.e. increasing the tensile strength reduces the ductility.

However, the 3hr-specimens are much tougher than the 17hr-specimens because the area under the former curves is greater than that of the latter curves. This indicates that the 3hr-specimens absorb more energy than the 17hr-specimens before failure. Toughness is defined as the total area under the stress-strain curve. It indicates the amount of energy absorbed before failure [2].

In the stress-strain curve, the 3hr-specimens displayed the typical aluminium alloys T4 condition characteristics while the 17hr-specimens displayed typical β"-optimised T6 condition characteristics. The 3hr-specimen with the best combination of yield strength and ductility is A3/520. Coincidentally A3/520 is hardest alloy after 3 hour annealing time.

Since the first peak hardness for this alloy has been attributed to GP-zones, then we can also speculate that the attained yield stress and ductility for all the 3 hour specimens is largely due to the GP-zones. The GP zones in Alloy A3 after 3 hours annealing time at 175°C were very fine and could only be seen at high magnification. The precipitates on the grain boundary and the PFZs adjacent to grain boundaries could be seen for alloy A12 . The 17hr-specimens recorded a much higher yield stress and corresponded to the peak hardness for alloy A12 and the 2nd peak hardness for A3. Since maximum hardness after 17hr annealing time is due to the formation of a very dense, β" microstructure, we can also argue that the higher yield strength is attributed to β".

- Yield stress rises with increasing volume fraction, UTS is not similarly affected.
- The annealing time of 17 hours improves both yield stress (0.2% proof stress) and UTS
- Very low volume fractions are desirable in terms of ductility

The deformation behaviour is seemingly controlled by the interaction of the 2nd phase particles for the 2 alloys. Deformation behaviour is controlled by interation of disloacations and precipitates.

Varying the aging condition would alter the density and size of precipitates so as to change the deformation behaviour.

The shape and magnitude of the stress strain curves of the two alloys depends on alloy composition and heat treatment. Below an explanation is given using 4 mechanisms to show why the yield strength is lower at lower ageing times and it is higher at higher ageing times.

- As GP zones and other precipitates are formed, it follows that there is a corresponding reduction of solute in the phase. The contribution of solute hardening to the overall

alloy strength therefore diminishes during ageing. It will reach a stable value when the phase reaches its equilibrium composition [12].

- As the GP zones nucleate and grow, there is an increase in the level of coherency strain hardening. This reaches a maximum when the average zone separation is about equal to the limiting radius of dislocation curvature. Coherency strain hardening is due to the resistance to dislocation motion provided by coherency strain fields [12].

- As the number and size of coherent precipitates increases, the role of chemical hardening becomes greater. However, as the precipitates reach a certain size, coherency starts to break down, and they can no longer be cut by dislocations [2,12].

- As new incoherent precipitates start to form, dispersion hardening becomes the dominant strengthening mechanism. At longer ageing times, these precipitates tend to coarsen, and the strengthening effect decreases. Note that the transition between chemical and dispersion hardening is rarely abrupt- the two mechanisms can operate within the same alloy. At higher ageing times and/or temperatures, precipitates become incoherent and dislocations are no longer able to cut through them. Instead, they must by-pass the precipitate by one of a number of possible mechanisms. These include bowing, climb and cross-slip. Dispersion hardening is due to the increase in applied stress required to by-pass an incoherent precipitate or particle [12].

- The overall ageing curve (read lower yield strength and higher yield strength at lower and higher ageing times respectively) is based on the 4 mechanisms listed above. . The first two mechanisms are roughly additive [12] while the latter two are competing mechanisms, so the overall strength will be a weighted average of the two.

4.7 Electrical Conductivity

The graphs (Figure 4-13, page 66) show that electrical conductivity for both A3 and A12 was generally lower at the beginning of the ageing process and continued to rise with increasing annealing time. This was true for both solution heat treatments i.e. for both there was a general positive gradient. The conductivity for A3 was higher than that of A12 (for both cases of solution heat treatment) for the first ~9 hours of annealing time. However, the conductivity of A12 became higher than that of A3 after ~9 to 11hours of annealing time. Put simply, when the alloys are in the under-aged condition, the conductivity of A3 is higher than that of A12 for both solution heat treatments. In the over-aged condition, the reverse is true. The conductivity of A12 overtook that of A3 at about 9 to 11 hours of ageing time. At the beginning of the ageing process, their conductivities are almost similar but at the end of the ageing process, the conductivity of A12 is much higher than that of A3. Note that the conductivity of A3/520 is lower than the conductivity of A3/570. Similarly, the conductivity of A12/520 is lower than that of A12/570.

Electrical conductivity measurements were only meant to estimate the total amount of solute atoms (Mg and Si) in the Aluminium lattice. Hence conductivity measurements were done to give us an idea about the solute atoms in solid solution. Solid Solution (SS) from the supersaturated Mg and Si greatly decreases conductivity. The more the SS, in the Al lattice the less the conductivity.

During ageing, the Si and Mg leaves the Al lattice to produce a coherent precipitate The precipitate does not interfere with conductivity as much as the SS atoms. As GP zones and other precipitates are formed, it follows that there is a corresponding reduction of solute in the phase and this explains why the conductivity was rising.

When the volume fraction is low and the particles are incoherent, they alloy should how have a high electrical conductivity approaching that of pure Aluminium [13].

TEM analysis of A12 and A3 led to the following conclusions (see Table 4-5 page 74):-

- After 3 hours of annealing time, A12/520 and A12/570 recorded a volume fraction (V.F) of 0.14% and 0.11% respectively as compared to A3/520 and A3/570 0.33%

and 0.48% respectively. Clearly this result shows that there was more precipitation in A3 than A12 at the beginning of the aging process. The higher the V.F, the more precipitation and hence the more the resistivity (i.e. less conductivity). The less the precipitation, (implied by low V.F) the less is the electrical resistivity (i.e. more conductivity). This scenario confirms earlier research pointing to the fact that at the beginning of ageing process the precipitation in Mg-rich alloys delays as compared to the precipitation in Si –rich alloys subjected to same heat treatments.

- After 17 hours annealing time, both A3/570 and A3/520 recorded a lower V.F as compared to A12/520 and A12/570 and this is the exact opposite of the 3 hours annealing time. This explains why the conductivity of A12 overtook that of A3.

- Comparing A3/520 A3/570 after 3 hours annealing time: V.F of A3/570 and A3/520 is 0.48% and 0.33% respectively. Indicator of more precipitation in A3/570 than A3/520. A3/570 has more resitivity (lower conductivity). A closer look at the conductivity curves also confirms this point. For the case of A12/520 and A12/570, they have almost equal precipitation after 3 hours annealing time and their conductivities is almost the same.

5 Chapter 5 CONCLUSIONS AND SUGGESTIONS FOR FURTHER WORK

5.1 Conclusions

- Alloy A3 (Si-rich alloy) was found to have the best combination of mechanical properties when it was subjected to a solution heat treatment temperature of 520°C for 10 minutes before quenching and storage at room temperature for 4 hours before it was aged at 175°C for 3 hours. Its Hardness was found to be 109 HV, yield strength = 219Mpa, ductility = 11% and ultimate tensile strength= 251Mpa. Hence a higher hardness for A3 was achieved using a lower solution heat temperature and time and shorter annealing time. This also produced the best ductility. This result is very significant for industry to design an alloy with better mechanical properties at low cost of production.

- The Si-rich alloy can be described has having typically very fine precipitate microstructure. The increase in hardness, yield strength and ductility are attributed GP-zones and β" phases. β" is the most effective hardening phase [3]. The reason for the hardening effect is the interface coherency in {001} type Al planes that produces a strong strain field around the precipitates, which slows the movement of dislocations [3]. A high number density of precipitates is responsible for high hardness.

- A3/520 is harder than A3/570 because the former contains slightly more particle number density, slightly lower cross-sectional area and slightly shorter needle lengths. Hence A3/520 has a slightly finer precipitate microstructure than A3/570.

- The shape and magnitude of the stress strain curves of the two alloys depends on alloy composition and heat treatment.

- The size of the new grain depends on the solution heat treatment temperature and the annealing time. Grain size increases with increase of solution heat treatment temperature. It also increases with increase in annealing time.

- The relationship between yield strength and grain size does not follow Hall-Petch equation especially when considering each solution heat treatment temperature at a time and at different annealing times. But when comparing grain sizes for the two solution heat treatments at the same annealing time, there is a weak follow up to Hall-Petch equation with an exception to A3/520/17h(YS=259Mpa) and A3/570/17h(YS=263Mpa).

- Tensile Strength and ductility are both dependent on the annealing time. At shorter annealing time, the tensile strength is less and ductility high and the reverse is true at higher annealing time.

- Yield strength is dependent on Si/Mg ratio especially at shorter annealing times. The higher the ratio, the better the yield strength.

- At shorter annealing time, yield strength also depends on solution heat treatment temperature. The lower the solution treatment temperature, the better the yield strength.

- To some extent, ductility depends on Si/Mg ratio. The higher the ratio the better the ductility. This is only valid at lower annealing time.

- Lower volume fractions are desirable in terms of ductility. Higher volume fractions are desirable for higher yield strength.

5.2 Suggestions for further work

- It will be of interest to repeat the tensile tests with similar specimens but must contain dispersoids. By adding dispersoids, the aluminium alloys will be able to withstand high temperatures without recrystallising. Recrystallisation may lead to a significant deterioration of material properties (strength loss, anisotropic properties/texture, increased tendency to weld-cracking, decreased corrosion

resistance and fracture toughness). Dispersoids (e.g. manganese and scandium) will pin the growing subgrains (recrystallisation nuclei), and this may lead to an improved recrystallisation resistance.

- We may try to vary the total sum of the solute elements, Mg and Si in the alloys, (i.e. Mg±Si) and then repeat the hardness measurements, electrical conductivity tests and tensile test experiments.

- Experiments involving Atom Probe Field Ion Microscopy (APFIM) on the clusters should be carried out to determine the characteristics of the atom clusters that make alloy A3/520 stronger than A3/570.

6 Bibliography

[1] John D. Verhoeven. *Fundamentals of Physical Metallurgy*. John Wiley & Sons,1975

[2] R. E. Smallman. *Modern Physical Metallurgy,* Fourth Edition. Butterworths

[3] Calin D. Marioara. *A TEM study of the Precipitates in a 6082 Al-Mg-Si Alloy System*. PhD Thesis, NTNU, 2000

[4] T. W. Clyne and P. J. Withers. *An Introduction to Metal Matrix Composites*. Cambridge University Press, 1993.

[5] Polmear I. J. *Light Alloys – Metallurgy of the light alloys*. Arnold, London, 1995.

[6] Parson, N.C., Liu, H.L.,. *Light Metals (Minerals, Metals and Materials Society*.).1998

[7] Edwards, G.A., Dunlop, G.L., Couper, M.J., 1994. *Proceedings of the 4th International Conference on Aluminium Alloys.*, *Vol 1*. 1994

[8] Zandbergen, H.W., Andersen, S.J., Janse, J. *Science* 227,1997

[9] Sigrun Haugen. β″*Phases as a Function of Alloy Composition in Al-Mg-Si Alloys*. Diploma Thesis, NTNU, 2002.

[10] http://aluminium.matter.org.uk/about.htm

[11] George E. Dieter*, Mechanical Metallurgy, Metric Editions*

[12] C.D Marioara, S. J. Andersen, R. Holmestad, *The influence of Alloy composition on precipitates of the Al-Mg-Si System*

[13] The 3rd International Conference on Aluminium alloys, their Physical and Mechanical properties Volume III, Norwegian Institute of Technology.

[14] http://info.lu.farmingdale.edu/depts/met/met205/index.html

[15] Matsuda et alActa

[16] Materiala: Vol 46 (1998); 3283-3298

[17] Acta Materiala Vol 49(2001); 321-328

[18] Anders G. Frøseth *Atomistic modelling of the Al-Mg-Si Alloy System*. PhD Thesis, NTNU, 2003

[19] The 3rd International Conference on Aluminium alloys, their Physical and Mechanical properties Volume II, Norwegian Institute of Technology.

[20] The 3rd International Conference on Aluminium alloys, their Physical and Mechanical properties Volume I, Norwegian Institute of Technology.

[21] M. J. Whelan et al. *Electron Microscopy of thin crystals*. Butterworths.

7 APPENDIX

7.1 The Al-Mg-Si Phase digram for Homogenanization

- The amounts of Mg and Si in commercial AA6xxx-alloys are of the same order of magnitude as the solid solubility in the range 450-580°C. The homogenisation temperature should be chosen so high that Mg_2Si and Si dissolve, but not so high that the alloy melts. This becomes increasingly difficult as the Mg- and Si-content of the alloy increases. Figure 7-1 (a) and Figure 7-1 (b) show phase diagrams.

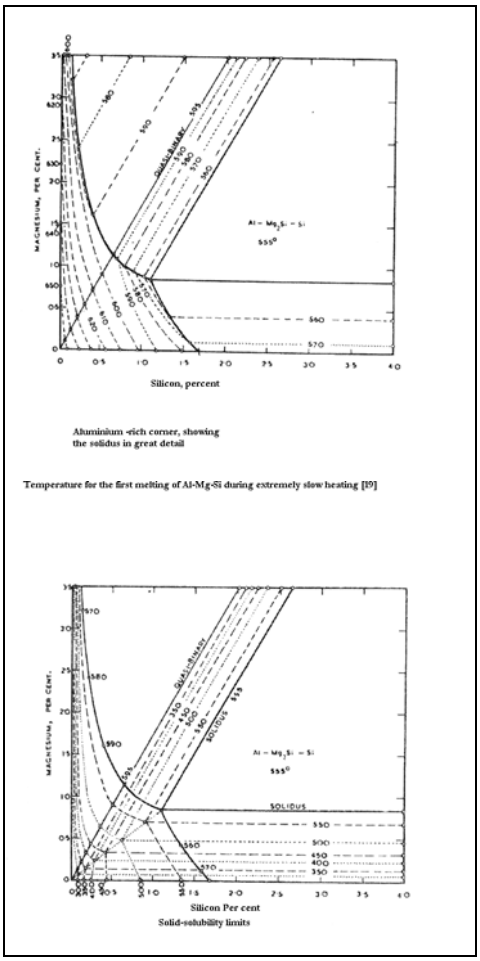

Figure 7-1 Solid Solubility limits for Al-Mg-Si [19]

7.2 GLOSSARY

Alloy: a solid comprising two or more elements that has metallic properties

Ageing: a change in the properties of certain metals and alloys that occurs at ambient or moderately elevated temperatures after hot working, heat treatment, or a cold working operation

Annealing: heating a solid at temperatures of generally one-half to two-thirds of the melting point on the Kelvin scale, followed by slow cooling. This process alloys some atomic rearrangement, removing some defects, and thereby improving the crystallinity of the solid.

Diffraction: the scattering of light from a regular array, producing constructive interference. In crystallography, diffraction of X-rays is observed from the regular and repeating arrays of atoms in a crystalline solid.

Dislocation: a type of one-dimensional (line) defect in a crystal. Movement of dislocations facilitates the motion of atoms in a crystal.

Ductile: the ability of a material to undergo changes in shape (plastic deformation), such as being drawn into wires, rather than breaking; a term often applied to metals. Ductility may be expressed as percent elongation or percent area reduction from a tensile test.

Elastic deformation: a temporary change in shape in response to a stress; a removal of the stress restores the original shape (contrast plastic deformation)

Electrical conductivity: the ability of a material to carry an electric current. It is also the reciprocal of resistivity. It has units of $ohm^{-1}cm^{-1}$.

Grain: a small crystalline region randomly oriented within the bulk crystal.

Grain boundary: the intersection of two grains within a crystal.

Microstructure: the arrangement of atoms on a scale of micrometers ($10^{-6}m$).

Nanostructure: the arrangement of atoms on a scale of nanometers ($10^{-9}m$)

Pinning: the process of preventing the movement of atoms or defects within a crystal.

Plastic deformation: the ability to re-shape a material because of the sliding of atomic planes in a crystal relative to one another (contrast elastic deformation).

Precipitation hardening: generation of a precipitate of an impurity phase within a host crystal that serves to roughen slip planes and makes the motion of dislocations more difficult. This process generally results in harder but more brittle materials.

Quenching: the process of quickly immersing a hot object in a cold medium like water or liquid nitrogen to lock in a particular structural arrangement of atoms.

Slip plane: a plane of atoms that is able to slide past an adjacent plane of atoms with relative ease.

Solid solution hardening: improving the hardness of a metal by adding impurity atoms that are either much larger or smaller than the host atoms. This process roughens the slip planes and makes the motion of dislocations more difficult.

Toughness: a measure of the energy absorbed before and during the fracture process: it is equal to the area under the tensile stress-strain curve. i.e. Toughness is the ability of a material to absorb energy during the plastic deformation. The area under the curve represents it from the unstrained state to the rupture point.

Young's Modulus (E): Young's Modulus also known as the Elasticity Modulus of a material is the ratio of the stress versus the strain within the Elastic region. This is usually found from the slope of the stress vs. strain curve.

Elasticity Modulus = Stress / Strain

This is a more generalized version of the Hook's law, similar to the spring constant.

YIELD POINT: The stress/strain point at which material behaviour changes from elastic to plastic is known as the Yield Point. In practice this is difficult to determine, the Offset Yield Point is used in tabulations of material properties. At the Offset Yield Point the sample has deformed plastically to an extent that will leave the material with a permanent strain of 0.002 (0.2%) when it is at zero stress. The stress, at which this occurs, is the Offset Yield Stress.

Resilience: Resilience is the capacity of a material to absorb energy when it is deformed elastically and then, upon unloading to have this energy recovered. The area under the curve in the elastic region represents it

7.3 Data from tensile test

Table 7-1 Tensile data